VERTICAL WATER ENTRY OF SOME OGIVES, CONES, AND CUSPS

John L. Baldwin

Naval Surface Weapons Center
Silver Spring, Maryland

21 March 1975

UNCLASSIFIED

SECURITY CLASSIFICATION OF THIS PAGE (When Data Entered)

REPORT DOCUMENTATION PAGE	READ INSTRUCTIONS BEFORE COMPLETING FORM
1. REPORT NUMBER: NSWC/WOL/TR 75-20	2. GOVT ACCESSION NO.
3. RECIPIENT'S CATALOG NUMBER: AD-A009 399	
4. TITLE (and Subtitle): Vertical Water Entry of Some Ogives, Cones, and Cusps	5. TYPE OF REPORT & PERIOD COVERED: interim
	6. PERFORMING ORG. REPORT NUMBER
7. AUTHOR(s): John L. Baldwin	8. CONTRACT OR GRANT NUMBER(s)
9. PERFORMING ORGANIZATION NAME AND ADDRESS: Naval Surface Weapons Center, White Oak Laboratory, Silver Spring, Maryland 20910	10. PROGRAM ELEMENT, PROJECT, TASK AREA & WORK UNIT NUMBERS: 61153N; ORD 035B-001/UR109-01-01
11. CONTROLLING OFFICE NAME AND ADDRESS	12. REPORT DATE: 21 March 1975
	13. NUMBER OF PAGES: 54
14. MONITORING AGENCY NAME & ADDRESS(if different from Controlling Office)	15. SECURITY CLASS. (of this report): Unclassified
	15a. DECLASSIFICATION/DOWNGRADING SCHEDULE

16. DISTRIBUTION STATEMENT (of this Report)

Approved for public release; distribution unlimited.

17. DISTRIBUTION STATEMENT (of the abstract entered in Block 20, if different from Report)

18. SUPPLEMENTARY NOTES

19. KEY WORDS (Continue on reverse side if necessary and identify by block number)

Ogives, Cusps, Cones, Water entry, Vertical, Drag, Added mass

20. ABSTRACT (Continue on reverse side if necessary and identify by block number)

An experimental investigation of the vertical water-entry deceleration of two ogive shapes and two cusp shapes is described. For each of these four shapes, the total drag coefficient and added mass are determined as functions of penetration distance. These results, combined with previous work, provide a display of possible values for maximum water-entry drag coefficient as a function of forebody fineness ratio.

DD FORM 1 JAN 73 1473 EDITION OF 1 NOV 65 IS OBSOLETE S/N 0102-014-6601

UNCLASSIFIED

SECURITY CLASSIFICATION OF THIS PAGE (When Data Entered)

NSWC/WOL/TR 75-20 21 March 1975

VERTICAL WATER ENTRY OF SOME OGIVES, CONES, AND CUSPS

This report is a result of the continuing effort of the Naval Surface Weapons Center in the understanding of water-entry phenomena. The research reported herein was supported entirely by NAVSEA Code 03512 under task ORD-035B-001/UR109-01-01. The author would like to acknowledge Dr. Thomas Pierce of NAVSEA for his advice and interest in this program.

ROBERT WILLIAMSON II
Captain, USN

V. C. D. Dawson
By direction

CONTENTS

ILLUSTRATIONS

CONTENTS (Cont.)

TABLES

LIST OF SYMBOLS

a	acceleration
A	area to which drag coefficients are related (πR²)
B	buoyancy
C_d	total drag coefficient
C_{ds}	steady-state drag coefficient
g	acceleration of gravity
m	total added mass $m = (m_1 + m_2)$
m_1	steady-state added mass
m_2	lost added mass
M	mass of model
r	surface radius
R	base radius
RC	resistance-capacitance time constant
S	depth (distance traveled after water contact)
t	time from impact
U	instantaneous velocity
U_o	model velocity at impact
V	volts
α	cone angle of ogive or cusp
β	swept angle of ogive or cusp
ρ	mass density of the fluid

INTRODUCTION

In the study of water-entry forces, the simplest experimental case to handle is the vertical entry of cones since the law of similitude allows prediction of the nature of several important parameters. An extensive experimental study of cone water entry has been completed at the Naval Surface Weapons Center and is reported in Reference (1). From an experimental and geometric viewpoint, the next simplest case is probably the vertical entry of ogives. An ogive is a body of revolution, the nose profile of which is formed by the single arc of a circle. One limit of this geometric family is the hemisphere, while the cone may be considered as a "straight ogive," separating the normal ogive (bulging) from the inverted ogive called a cusp (hollow). This simple geometric family has received very little attention from experimenters in water entry with the exception of the ogives tested by Majer (Ref. (2)), and the hemisphere which has received considerable experimental and mathematical consideration by several investigators.

As the tests of the vertical entry of cones were being conducted at the Naval Surface Weapons Center, and the data were being reduced, speculation developed as to the effects of profile curvature upon the water-entry characteristics of various shapes. A short series of tests was conducted as a preliminary investigation to answer some of these speculations and to extend some of the results obtained for cones to other simple shapes (ogives).

TEST PROCEDURE

The test procedure was in principle identical to that reported in Reference (1) for cones, and the data contained in Reference (1) are extensively used in this report. The experiments were conducted in the Pilot Hydroballistics Facility at Naval Surface Weapons Center, Figure 1. The model, containing a single axially mounted crystal accelerometer, was launched from an air gun (velocity, 30 feet per second and higher) or dropped through a tube, such that normal impact with the surface of the water resulted. A cable (trailing wire) connected the accelerometer within the model to stationary electronics. The output of the gage after amplification was photographically recorded using a CRT oscilloscope. As the model neared the water surface, a trigger screen was interrupted, causing a microsecond strobe lamp to produce three flashes equally spaced in time, thus exposing the film in an open plate camera. Located beside the camera was a photo-pickup that converted the light from the strobe into voltage that was mixed with the accelerometer output to the oscilloscope. The arrangement of equipment for these tests is shown in Figure 2. The height of the trigger was adjusted such that the reflection of the model on the water surface was photographed, as well as the model, thus defining the surface to be impacted. This technique resulted in two photographs, one

1. J. L. Baldwin, "Vertical Water Entry of Cones," NOLTR 71-25 of 11 Feb 1971

2. A. Weible, "The Penetration Resistance of Bodies with various Head Forms at Perpendicular Impact on Water," German Avia Res. Rpt No. 4541, Naval Research Laboratory Transl. No. 286, revised (1952)

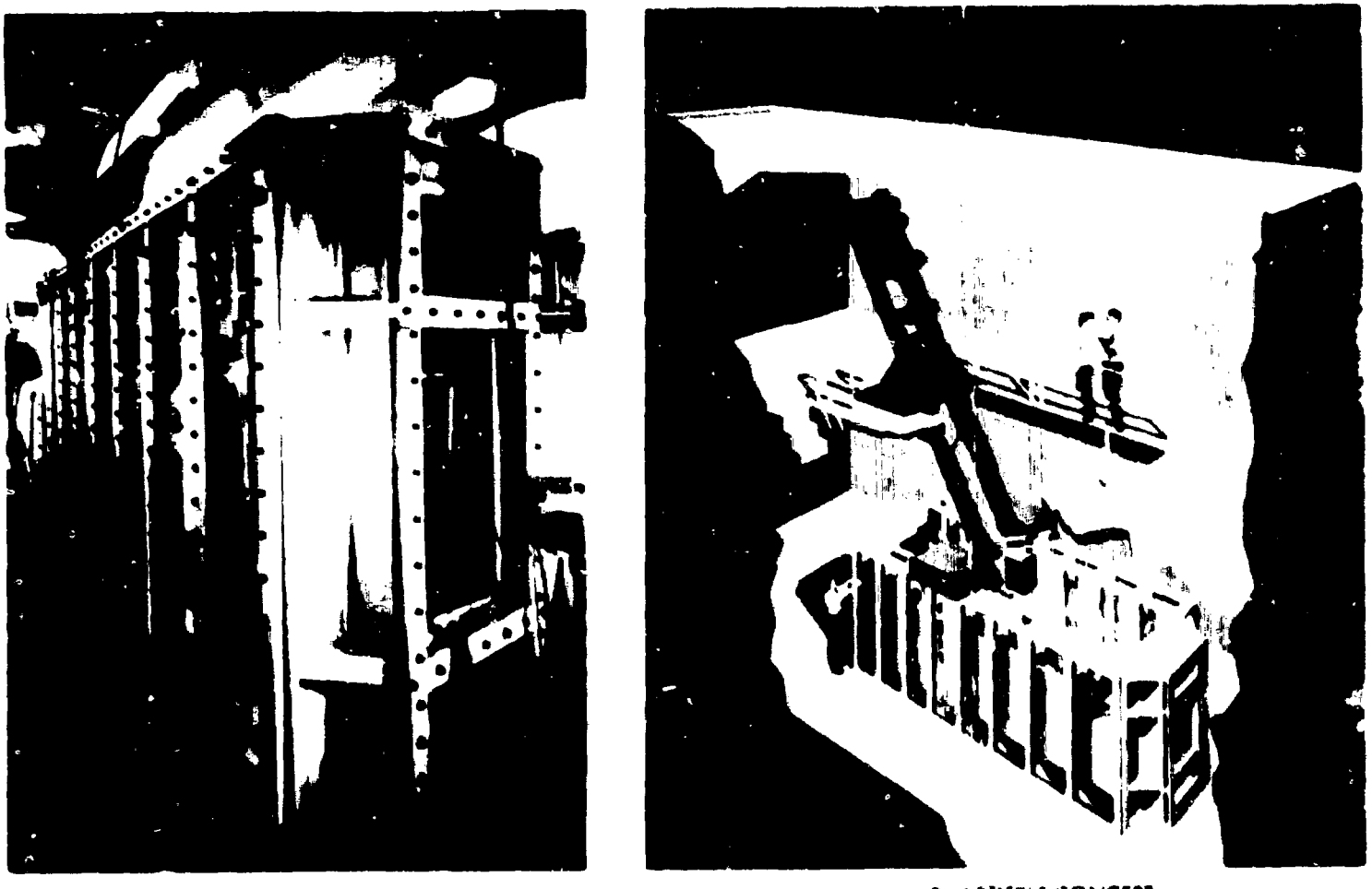

A. PHOTOGRAPH

B. ARTIST'S CONCEPT

FIG. 1 HYDROBALLISTICS PILOT TANK

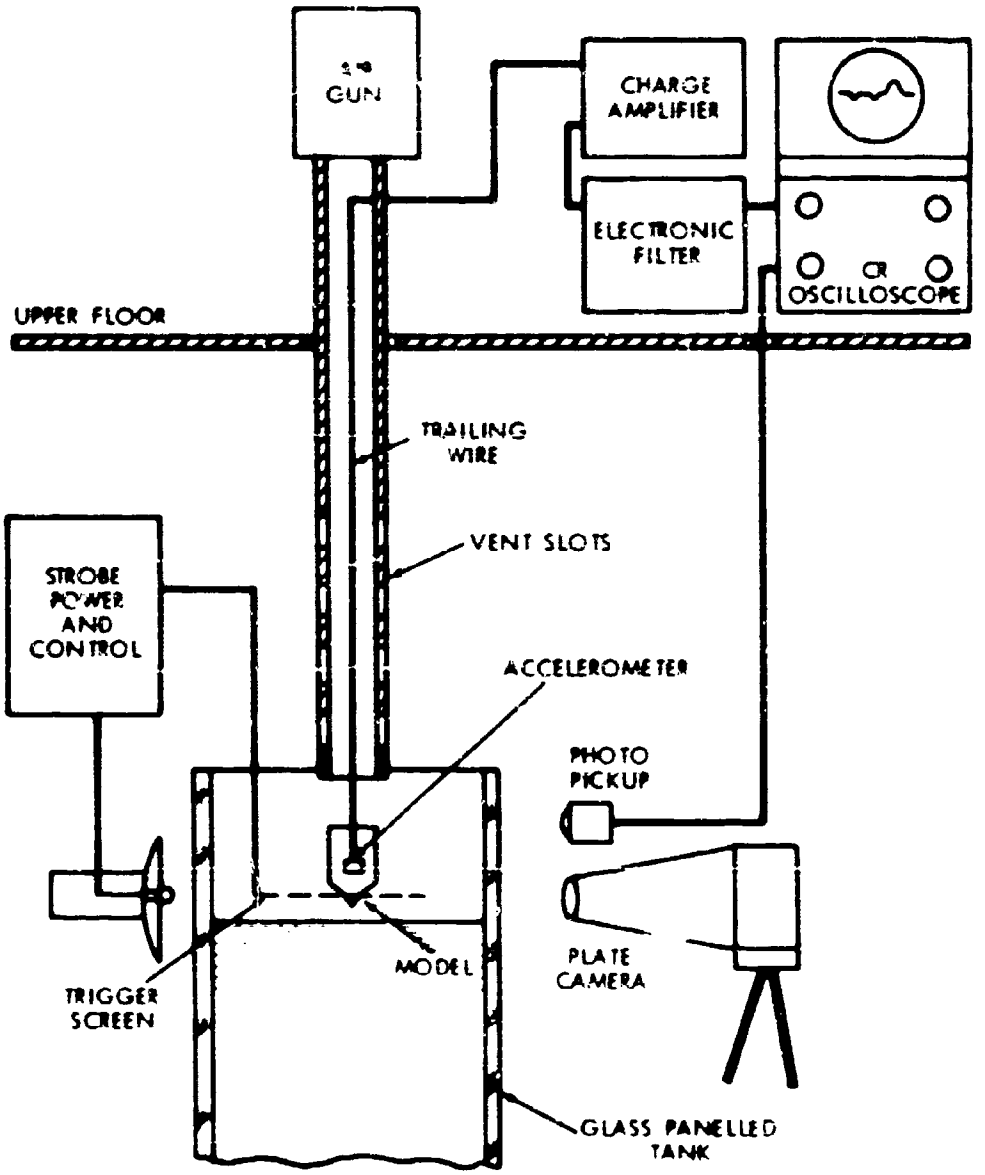

FIG. 2 TEST EQUIPMENT SCHEMATIC

showing the model, generally above the water surface, at three points in time; and the other showing the voltage output of the accelerometer, and the time of each exposure on a common time base, displayed on an oscilloscope. Figure 3 shows two samples of these data. Additional data samples are given in Appendix A.

The models used in this test series were simple three-inch-diameter-ogive cylinders in which the accelerometer was mounted. One of the gages used was not waterproof and required a seal nut that increased the total model weight by about 100 grams. Offsets of each nose were measured to an accuracy of ±.001-inch in both station and radius and are included in Appendix B. The nose shapes calculated from the measurements did not closely agree with the nominal values. The greatest difference was the 90/30° ogive which seemed to be an 88.42/32. These errors were noted but no corrections were made during the data reduction.

Only three accelerometers were used during the entire test series (the same gages used in the tests reported in Reference (1)), a high-capacitance, high-impedance, multiple-crystal gage; and two similar quartz gages with internal electronics responsible for low-output impedance. The capacitance of the multiple-crystal gage reduced the relative error caused by changes in capacitance in the cable (trailing wire) due to acceleration and other loads. The multiple crystal accelerometer was used with a charge amplifier to increase the system RC time constant when a maximum acceleration of less than 30g was expected. An electronic filter was also often used.

The gages, scopes, filters, and charge amplifier were calibrated as a system. Three methods of calibration were used for each gage and electronics combination employed in the test series. Several combinations were recalibrated during the test series. The three calibration methods were: (1) shaker table with optical measurement of displacement; (2) shaker table with comparison with a standard gage; and (3) a one-g drop.

In the one-g drop test, the gage and model were held by a short length of nichrome wire. A high current electric source was applied to the wire, causing rapid melting and quick release. This step pulse of one-g was used to determine the leakage rate of the gage-electronic system, as well as determining the gage constant.

The gage constants used for each system were the simple average of the gage constants determined from all calibration techniques.

RANGE OF VARIABLES TESTED

In the test series, the effects of model shape and entry velocity were studied. Four shapes were tested; two convex

* ogive nomenclature is shown in Figure 5

FIG. 3 SAMPLE OF TEST DATA

ogives and two cusps. The details of these models are shown in Appendix B. The velocity range studied was from 13 feet per second to 80 feet per second. A total of thirty tests were made.

DATA REDUCTION AND DISCUSSION

The "a priori" assumption made in the data reduction was that the external forces depend only upon size, geometry, actual velocity, and distance below the water surface. Additionally, it was assumed that: (1) buoyancy force is calculated from original water surface; (2) friction drag coefficient is constant for all conditions.

The preliminary data reduction was done manually and involved changing the photographic records to digital form. The photographic information on the plate camera and oscilloscope records was reduced to numbers as follows: the plate camera photograph was used to determine the impact velocity and to locate the water surface relative to the oscilloscope trace. The distance the model advanced between flashes was computed using the diameter of the model as a reference dimension. The time between flashes was measured by an electric counter. The distance from the reference picture was measured (if possible) to a point halfway between the picture and the matching reflection. Again, the model diameter was used as the reference length.

The readings of the oscilloscope records were made using a film reader or toolmaker's microscope in the following order: the distance of a vertical centimeter was read to determine the scale factor; next, the pip relating the model's position with the water was read; and then a series of points along the trace were read. Both components of each point were recorded.

The numbers obtained from the pictures, along with recorded information such as model diameter, weight, and scope gain, were entered into a time-shared digital computer.

The acceleration time data were converted to English engineering units for computations. The coordinate axes were shifted such that zero acceleration occurred just before impact and that time zero occurred at water contact. The following correction for leakage was then applied:

$$\frac{dU}{dt}\ (\text{True}) = \frac{dU}{dt}\ (\text{read}) + \frac{1}{RC}\int_0^t \frac{dU}{dt}\ (\text{read})\,dt$$

The acceleration coordinate axis was shifted such that + one g occurred just before the water contact. The velocity and distance were then determined for each data point using trapezoidal integration. The values related to water-entry effects were then computed.

The equation relating the momentum just before first contact with the momentum at some later time is given as Equation (1), and the force equation is given as Equation (2).

$$U_o M - U(M+m_1) = \int_0^t B\,dt - Mgt + \frac{\rho}{2}\int_0^t C_{ds} A U^2 dt \qquad (1)$$

$$-\frac{dU}{dt}(M+m_1) - U\frac{dm_1}{dt} = B - Mg + \frac{\rho}{2} C_{ds} A U^2 \qquad (2)$$

Substituting $U^2 \frac{dm_1}{dS}$ for the second term of Equation (2) and rearranging terms gives:

$$-\frac{dU}{dt}(M+m_1) - B + Mg = \frac{dm_1}{dS} U^2 + \frac{\rho}{2} C_{ds}(S) A U^2 \qquad (3)$$

If the total drag coefficient is defined as

$$C_d(S) = \frac{2}{\rho A}\frac{dm_1}{dS} + C_{ds} \qquad (4)$$

then Equation (3) may be rewritten as

$$-\frac{dU}{dt}(M+m_1) - B + Mg = \frac{1}{2}\rho\, C_d(S) A U^2 \qquad (5)$$

In Equation (3) there are two unknowns, $m_1(t)$ and $C_{ds}(t)$. One method of solution is to test models with two different masses and then solve simultaneously for $m(t)$ and $C_{ds}(t)$. This technique was suggested by Dr. Arnold E. Seigel of NAVSURFWPNCEN.

An attempt was made to separate $m_1(t)$ from $C_{ds}(t)$ for cones during vertical entry (Ref. (3)). The results indicated that C_{ds} was equal to zero until the base of the cone passed the original water surface. For deeper penetrations large scatter occurred in the values of C_{ds} making definitive results impossible. The use of models with single mass for each geometric shape during these tests of ogives and cusps prevented the use of the simultaneous solution method of separation.

Being unable to separate the added mass, $m_1(t)$ from the steady-state drag coefficient (C_{ds}), it was decided to combine them. The usefulness of this approximation and resulting errors were obtained from Equations (1) through (5) as follows:

3. "An Experimental Investigation of Water Entry", thesis by John L. Baldwin for Ph.D., 19 May 1972

The added mass (m_1) is the added mass of the steady-state flow field of the water entry body and the water impact force $U\frac{dm_1}{dt}$ is due to the establishment of this flow field. Hence, the value of added mass should approach a steady valve when the surface has been passed. Changes in added mass due to cavity collapse occurred at depths much greater than studied in these experiments.

Buoyancy and weight require no interruptive comments. Both are usually neglected during high-speed entry or may be easily estimated.

Losses in momentum relative to the body were expressed in Equation (1) as the integral of steady-state drag coefficient (C_{ds}). Cavity formation and viscous wakes contributed to C_{ds}. Hence, C_{ds} remained small until cavity or wake formation began and then increased to the value obtained in steady-state water tunnel experiments. The importance of these losses were estimated by the:

1. Observation from Equation (3) that the steady-state drag coefficient could be represented by the derivative of lost added mass (m_2).

$$\frac{\rho}{2} C_{ds}\ (S)\ A\ U^2 = \frac{dm_2}{ds} U^2 = \frac{dm_2}{dt} U \qquad (6)$$

2. Substitution of Equation (6) into Equation (1) and the application of integration by parts obtained Equation (7).

$$U_o\ M-U\ (M + m_1) = \int_{t_o}^{t} B dt - Mgt + Um_2 - \int_{t_o}^{t} m_2(t)\frac{du}{d\tilde{t}}\, dt \qquad (7)$$

3. Evaluation of the last term assuming that m_2 was zero from t_o to t_1 and then a monotonic function from t_1 to t and that U was also a monotonic function

$$\int_o^t m_2(t)\ \frac{dU}{dt}\, dt = m_2\, \overline{\Delta U}$$

Equation (8) was obtained by the combination of the last two terms of Equation (7)

$$m_2\ (U - \Delta\bar{U}) = m_2\ U(1 - \frac{\Delta\bar{U}}{U}) \gtrless m_2\ U(1 - \frac{\Delta U}{U}) \qquad (8)$$

Where $\frac{\Delta U}{U}$ was the maximum error caused by the approximation

$$\int_o^t \frac{\rho}{2} C_{ds} A U^2 dt = Um_2$$

Note that ΔU is the change in speed from time (t_1) to time (t). Then Equations (1) through (5) were approximated by Equations (9) through (13) where $m = (m_1 + m_2)$

$$U_o M - U (M+m) = \int_o^t B dt - Mgt \tag{9}$$

$$- \frac{dU}{dt} (M+m) - U \frac{dm}{dt} = B - Mg \tag{10}$$

$$- \frac{dU}{dt} (M+m) - B + Mg = \frac{dm}{ds} U^2 \tag{11}$$

$$C_d(S) = \frac{2}{\rho A} \frac{dm}{ds} \tag{12}$$

$$- \frac{dU}{dt} (M+m) - B + Mg = \frac{1}{2} \rho C_d(S) AU^2 \tag{13}$$

When buoyancy and weight could be neglected, the instantaneous velocity was estimated by Equation (14) obtained from Equation (9)

$$U = \frac{M}{M+m} U_o \tag{14}$$

and the instantaneous model acceleration was estimated by Equation (15) obtained from Equations (13) and (14)

$$- \frac{dU}{dt} = \frac{1}{2} \rho C_d(S) A \frac{M^2}{(M+m)^3} U_o^2 \tag{15}$$

where the values of $C_d(S)$ and m are given in Appendix D. For weapon diameters other than three inches the values of added mass given must be multiplied by

$$\left(\frac{\text{Weapon Diameter in Inches}}{3} \right)^3$$

The experimental data consisted of the acceleration-time function $\frac{dU}{dt}$, initial velocity U_o and the time of water contact t_o. Trapezoidal rule integration of the acceleration-time function $\frac{dU}{dt}$ produced the velocity function (U). In like manner the distance function (S) was obtained by integration of the velocity function. The buoyancy force (B) was computed as the weight of water displaced by the model below the original water surface; i.e., no allowance was made for the cavity. The total drag coefficient was then computed using Equation (13); with the added mass (m) initially chosen equal to zero. Next the added mass was computed using Equation (12). The total drag coefficient was then recomputed using the last computed value of added mass. Then a new value of added mass was computed from the last value of total drag coefficient. The calculations were terminated after four iterations.

For easy comparison of the results for each shape, it was desirable to compute the final data at stations rather than at arbitrarily read data points. Sixteen stations were equally spaced between water contact and the depth at which the total drag coefficient had its maximum value. At deeper depths, the distance between stations were one, two or five times larger than the standard distance.

The values of velocity, time and acceleration were computed at each station by interpolation and the final data reduction continued as before using Equations (13) and (12) for four iterations. The computer program used to reduce the data was written in BASIC and is included in Appendix C.

The errors induced in the results by combining m_1 and m_2 were estimated by comparing the results of two assumed functions:

(1) $\frac{dm}{ds} = 0$ for all time

(2) $\frac{dm_2}{ds} = 0$ from water contact until the total drag coefficient became maximum and then a step to $\frac{dm_2}{ds}$ = maximum final value as shown by the dotted lines on Figure 4.

In these experiments the worst case was the maximum penetration of the 90/-30 cusp. At a penetration of four inches, the difference in the value of total mass (M + m) was less than 4.2 percent. The use of total added mass (m) caused an error in the calculated values of total drag coefficient of seven percent for this case. At deeper depths the error would continue to increase. Therefore, if Equations (1) through (5) are to be used after water impact a division of total added mass should be made. This division

CUSP

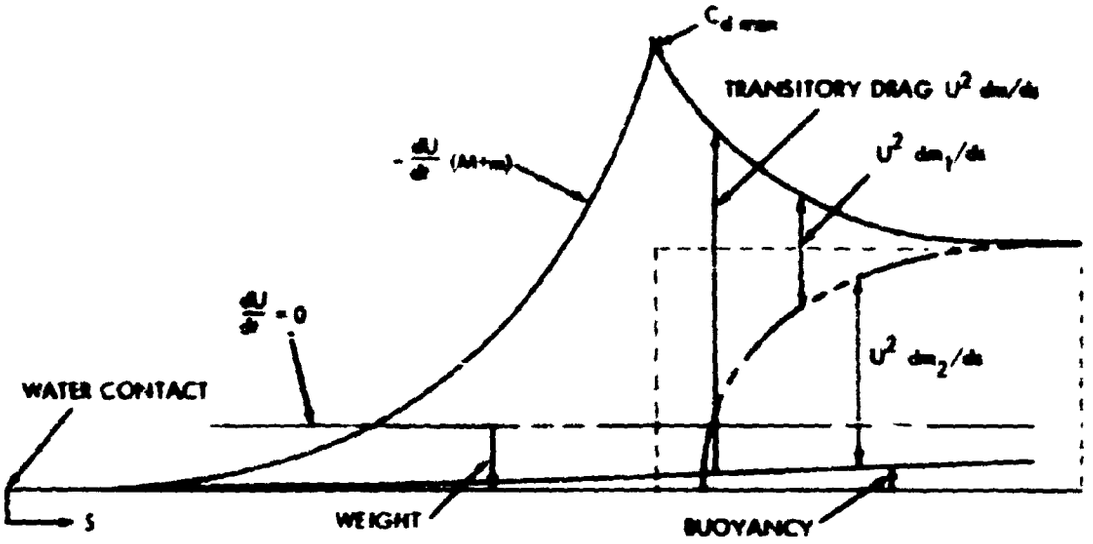

OGIVE

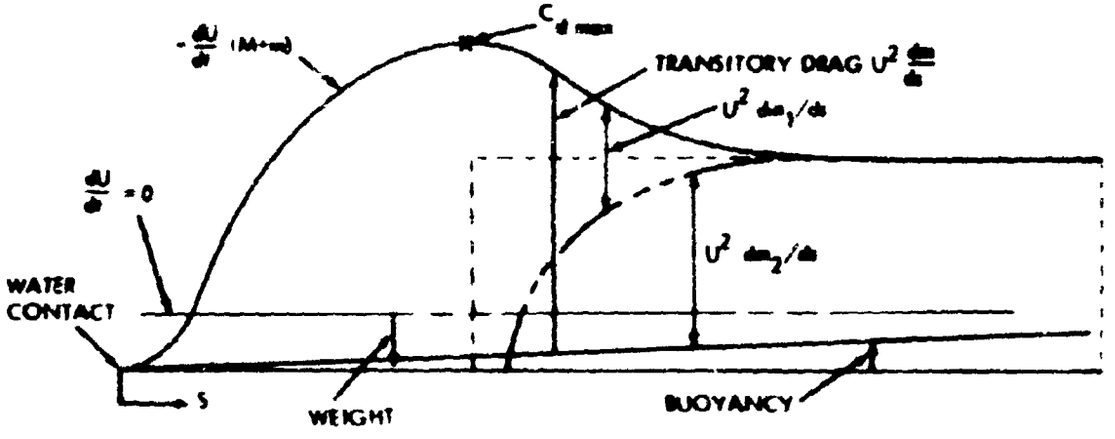

FIG. 4 FORCE MODEL VS DEPTH

must be arbitrary at this time because of the lack of data or quantitative theory. It is suggested that a suitable division can be made by a quarter ellipse beginning at the start of cavity formation and continuing for one body diameter. For bodies of moderate or large relative mass, the errors caused by a wrong division are small and noncumulative. The 90/-30 cusp model had a relative mass of .128 lbm/inches^3 which was about 1/2 to 1/10 the relative mass of common water-entry devices. Also, this worst case had a high final value of C_d which accentuated percent differences caused by different divisions. Therefore, for most cases the suggested division should be accurate to within five percent as would most other divisions beginning during early cavity formation.

GEOMETRY

There seems to be no standard method used in the literature to define ogive shapes. An ogive shape is a pointed body formed by rotating a circular arc. If the water-impact forces do indeed depend chiefly upon the geometry of the body, the shape will have to be defined more precisely. The method chosen for use in this report uses two angles and one reference length. One angle is the tip angle (α) of a cone of the same length and base as the ogive and the other angle (β) is the angle subtended by the arc. The base diameter is used as the reference length. The tip angle, base angle, slopes, and radii are all easily computed for both normal ogives and inverse ogives (cusps), as shown in Figure 5. Note that in Figure 5 the inclusion of a minus sign with the swept angle β changes the ogive to the cusp. An inspection of the computer program shows a continuing similarity in the geometric equations. The only difference, if any, is a minus sign for the cusp shape. The swept radius r is one parameter that has the same equation for both shapes.

$$r = R/(2 \sin(\alpha/2) \sin(\beta/2))$$

In the comparison of the results for different ogives, it is often possible to relate the forces to the base area of a tangent ogive. A method for computing the ratio between the base area of a secant ogive and corresponding tangent ogive is shown in Figure 6. As a basis for this comparison, the nomenclature must be such that the actual tip angle remains constant.

In this report, it is assumed that the tangent ogive is a limit of this geometric family of shapes. This implies that the swept angle may not be larger than the cone angle. It is also defined that the limit case for cusps is when the swept angle is equal to the cone angle. For cone angles of 90 degrees or more, this definition merely states that the base angle cannot be negative.

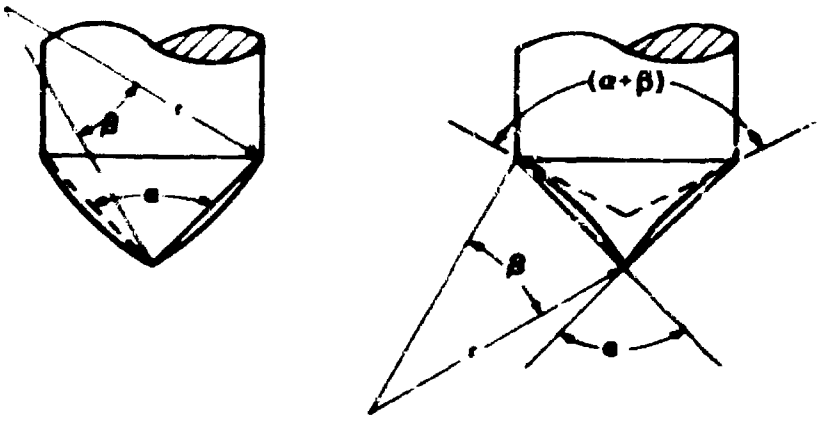

OGIVE	PROPERTY	CUSP
α/β	"NAME"	$\alpha/-\beta$
$\alpha+\beta$	TIP ANGLE	$\alpha-\beta$
$\alpha-\beta$	BASE ANGLE	$\alpha+\beta$

FIG. 5 OGIVE GEOMETRY

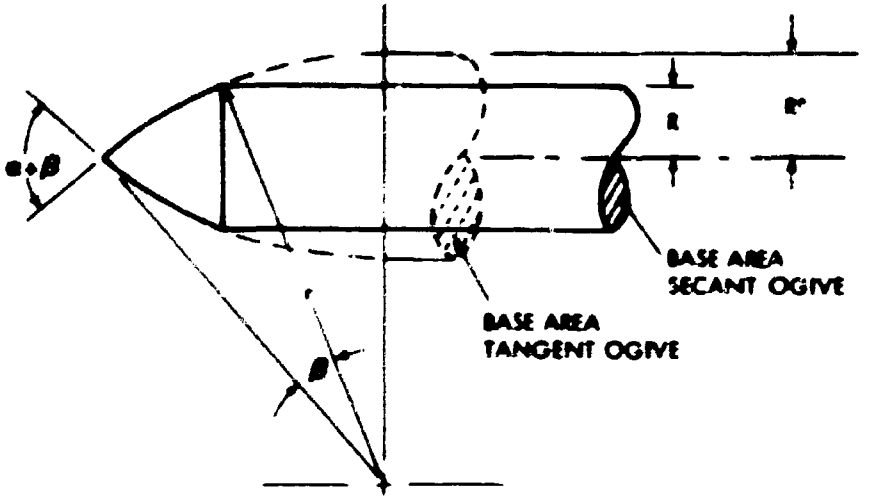

BASE AREA RATIO = $(R/R^*)^2$

$$(R/R^*)^2 = \left(\frac{2\sin^2\frac{\alpha}{2}\sin\frac{\beta}{2}}{1-\cos\frac{\alpha+\beta}{2}}\right)^2$$

FIG. 6 BASE AREA COMPARISON OF SECANT AND TANGENT OGIVES

RESULTS AND CONCLUSIONS

It is possible to compare the results of various tests of convex-ogive shapes by relating the drag coefficient to the base area of a tangent ogive of equal tip angle. This technique requires the assumption that separation occurs ahead of the base of the ogive tested or at least at a depth greater than that at which Cd_{max} occurs. Several separate tests were conducted on the convex ogives to determine the relationship between separation and acceleration. The entry of the 60/42.6 ogive is shown in Figure 7 which consists of strips from several high-speed movies and a representative acceleration trace. These photographs show that separation on the 60/42.6 ogive occurs at 85 percent of the nose length. Tests on the 90/30 ogive showed separation at the nose base at about 120 percent of the depth associated with Cd_{max}. The results of Cd_{max} for both shapes were reduced to the tangent ogive case and are given in Figure 8. Also shown are the values given in Reference (2) and some unpublished data from tests at the Naval Surface Weapons Center. Friction is included in the plotted data.

The relationship between total drag coefficient and velocity was investigated by normalizing the values of Cd_{max} and performing a least square fit to obtain:

$$\text{For the ogives } Cd_{max} = 1.013 - .00031\ U_c$$

$$\text{For the cusps } Cd_{max} = 1.014 - .00041\ U_c$$

Therefore, the total drag coefficient may be considered independent of velocity over the range of shapes and velocities considered. In addition, the entire drag coefficient-depth history seems to be independent of velocity (Appendix D). This conclusion is in agreement with the results for cones reported in Reference (1).

The added mass curves obtained for these ogives agree in form with the results obtained for cones (Appendix D and Reference (1)). Pointwise, values are also in substantial agreement, but not for equal cone angles (lengths). For example, the added mass associated with a 90/-30 cusp is in better agreement with the added mass associated with a 120-degree cone than with a 90-degree cone.

The tests demonstrated a strong dependence of the maximum drag coefficient upon the nose shape. The drag coefficient vs depth histories of a cusp, cone, and ogive of equal lengths are shown in Figure 9. It is seen that the cusp has twice the maximum drag coefficient of the cone, and that the ogive is slightly over half that of the cone.

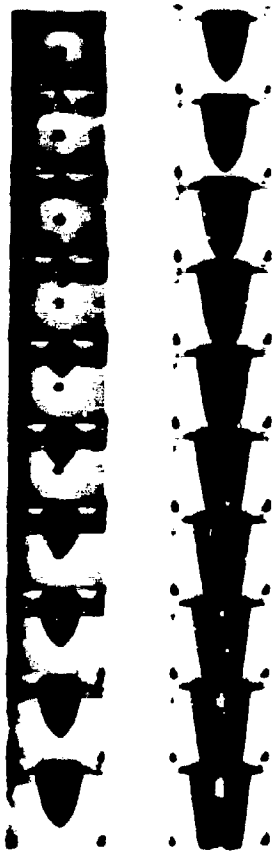

SHOT NUMBER 2075

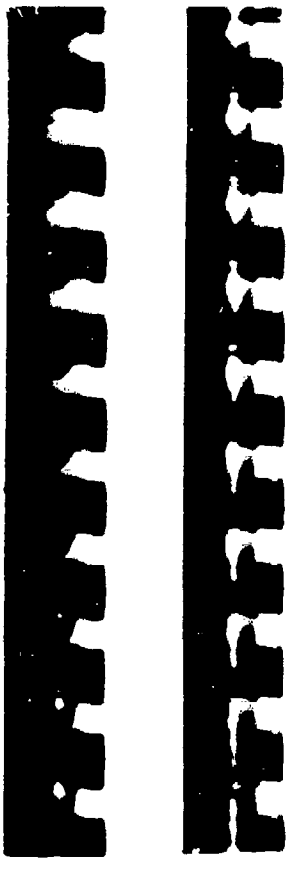

SHOT NUMBER 2076
(NO TRACE)

BOTH CAMERA SPEEDS APPROX. 1200 FPS

SYNCED STROBE ILLUMINATION

DISCONTINUITY IN TRACE CAUSED BY STROBE FLASH

SCOPE SWEEP 0.001 SEC CM

FIG. 7 UNDERWATER PICTURES AND COUPLED ACCELEROMETER TRACE FOR A 60-43 OGIVE ENTERING WATER AT APPROXIMATELY 70 FEET PER SECOND

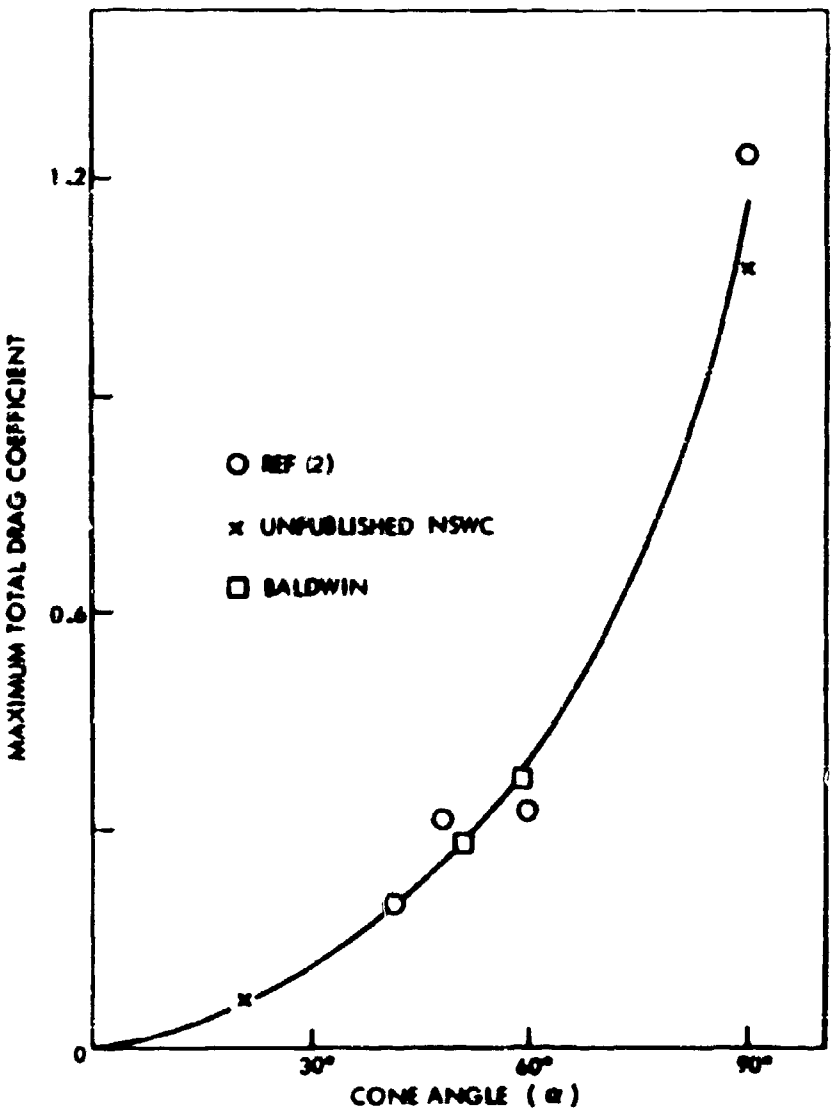

FIG. 8 MAXIMUM TOTAL DRAG COEFFICIENT OF TANGENT OGIVES

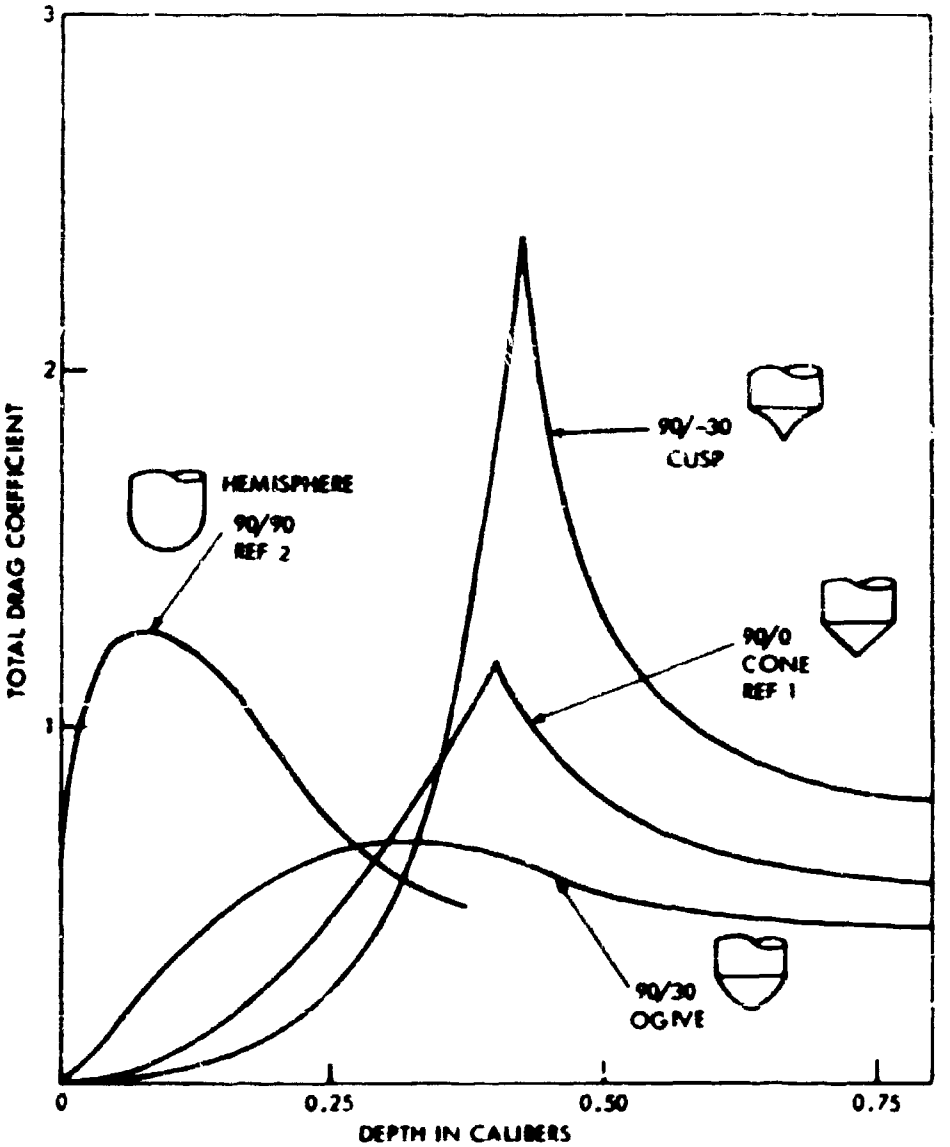

FIG. 9 TOTAL DRAG COEFFICIENT vs DEPTH FOR EQUAL LENGTH NOSE SHAPES

Also of interest is that the relatively slight curvature of the 90/30 ogive has changed the basic forcing function from concave upward, which a cone always has, to convex. The data regarding the hemisphere was taken from Reference (2) for comparison. These values are typical and not those of limit, or optimum configurations. It should also be noted that, in general, the steady-state drag coefficient is in the same relative order as the maximum drag coefficient, although this result is not true for the hemisphere.

The variation of maximum total drag coefficient Cd_{max} with changes in swept angle is shown in Figure 10. Curves are given that define the possible Cd_{max} values for shapes with a 90-degree cone angle (1-caliber length) and a 60-degree cone angle (1.73-caliber length). In addition, the probable curve for a 30-degree cone angle is illustrated. Also included are the geometric limit curves for this family, and the curve of minimum drag coefficients.

It is interesting to note that the ogive limit curve is a direct copy of Figure 8. This is due to equivalence of cone angle and swept angle in the case of tangent ogives. The scarcity of experimental data prevents the exact determination of these curves, particularly the cusp limit curve; however, the basic curve shapes seem to be established. In order to estimate a curve such as the 30-degree cone angle, the value of Cd_{max} is obtained for the cone shape from Reference (1) and plotted at zero swept angles equal to plus or minus the cone angle. Then a curve is faired between these three points such that it is a family member of the previously plotted experimental curves.

If sufficient data were available, it would be possible to divide the area between the cusp limit curve and ogive limit curve into two regions by a separation line. Shapes located between this separation line and the cusp limit curve would be fully wetted during entry. For all other ogives, separation would occur on the forebody; therefore, their drag coefficients could be determined from drag coefficient values of tangent ogives by simple geometric means. It is believed that this region would include most shapes of practical interest. One speculation is that the line of minimums is common with the separation line.

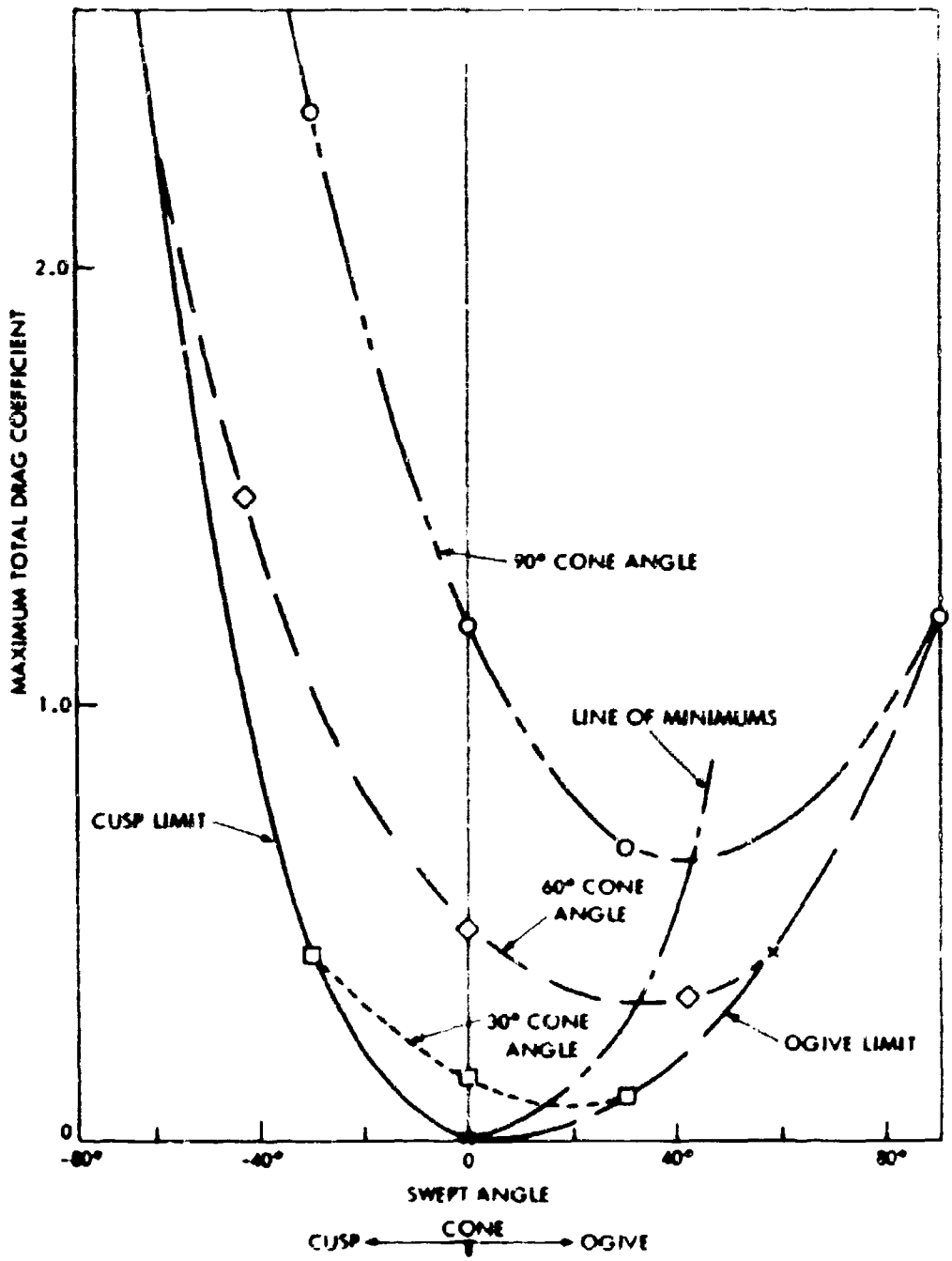

FIG. 10 MAXIMUM TOTAL DRAG COEFFICIENT FOR CUSPS, CONES AND OGIVES

APPENDIX A

The original data from several tests form this appendix. These particular tests were selected to provide information at separate velocities for each of the four shapes tested. The shot numbers, weight, gage constants, and other necessary numeric values are given in Table A-1. The remainder of this appendix contains optical copies of the original data photographs.

Table A-1

Numerical Constants

Shot No.	Shape	Weight (lbs)	Gage Constant ($ft/sec^2/V$)	Time Constant (sec)	Scope Gain (V/cm)	Scope Sweep (sec/cm)
2053*	60/43	4.34	18.7	.2	2.0	.005
2071	60/43	4.34	2609	.009	0.1	.001
2073*	60/43	4.34	2609	.009	0.1	.001
2051	90/30	3.64	3138	.75	.01	.005
2068	90/30	3.85	2609	.009	0.2	.001
2065	60/-43	3.81	2609	.009	0.2	.001
2066	60/-43	3.81	2609	.009	0.5	.001
2503	60/-43	3.57	2809	.08	.02	.005
2044	90/-30	3.46	3138	.75	.05	.005
2064	90/-30	3.70	2609	.009	0.5	.001

*Shown in Figure 3.

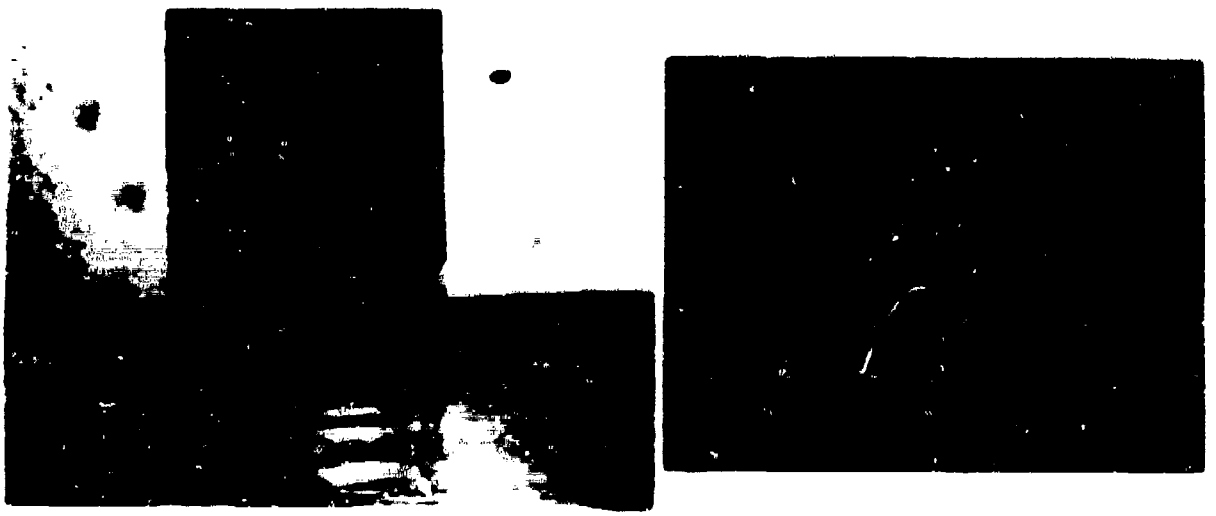

2051

2071

FIG. A-1 ORIGINAL DATA - TESTS 2051, 2071

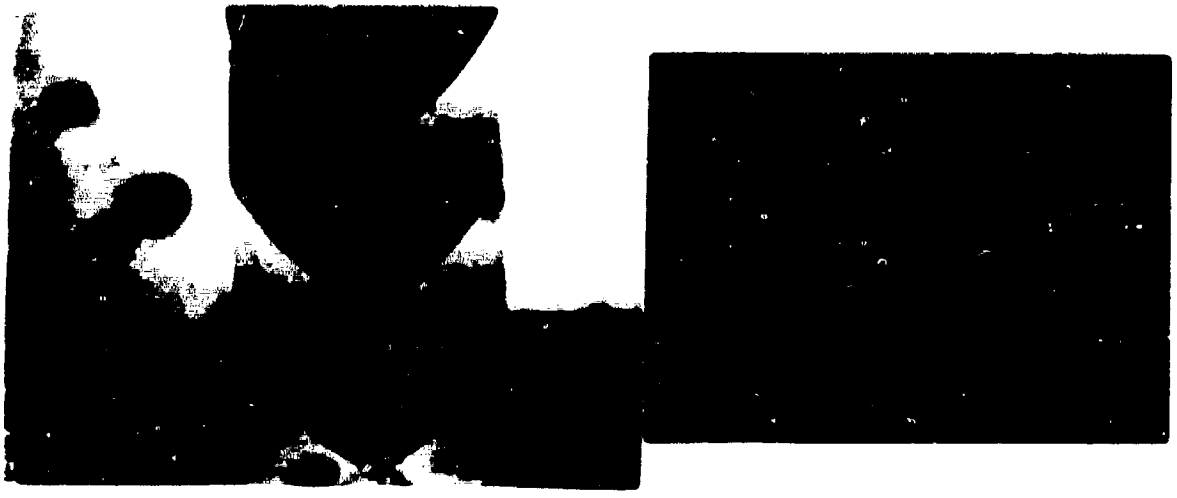

2068

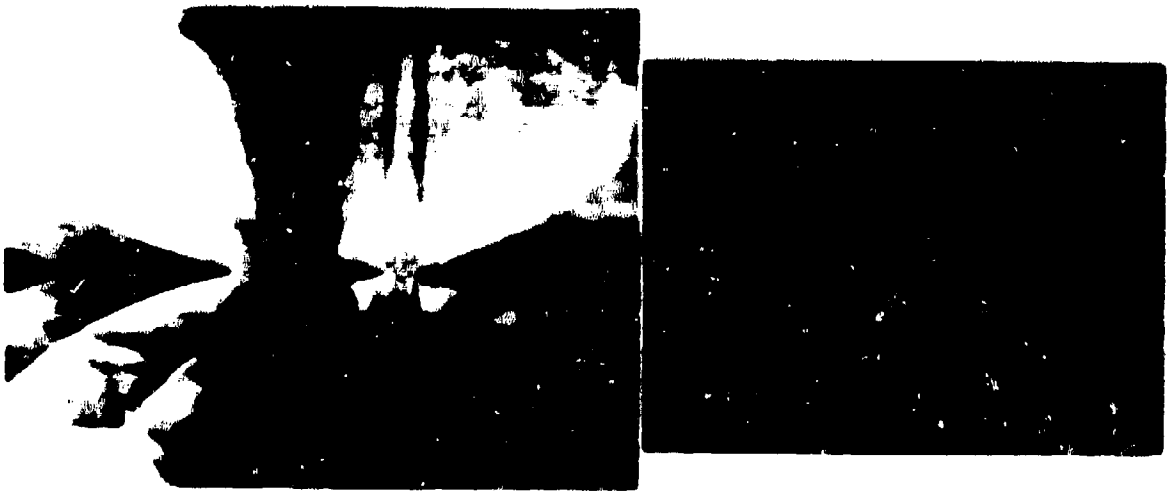

21503

FIG. A-2 ORIGINAL DATA - TESTS 2068, 21503

2065

2066

FIG. A-3 ORIGINAL DATA - TESTS 2065 2066

2044

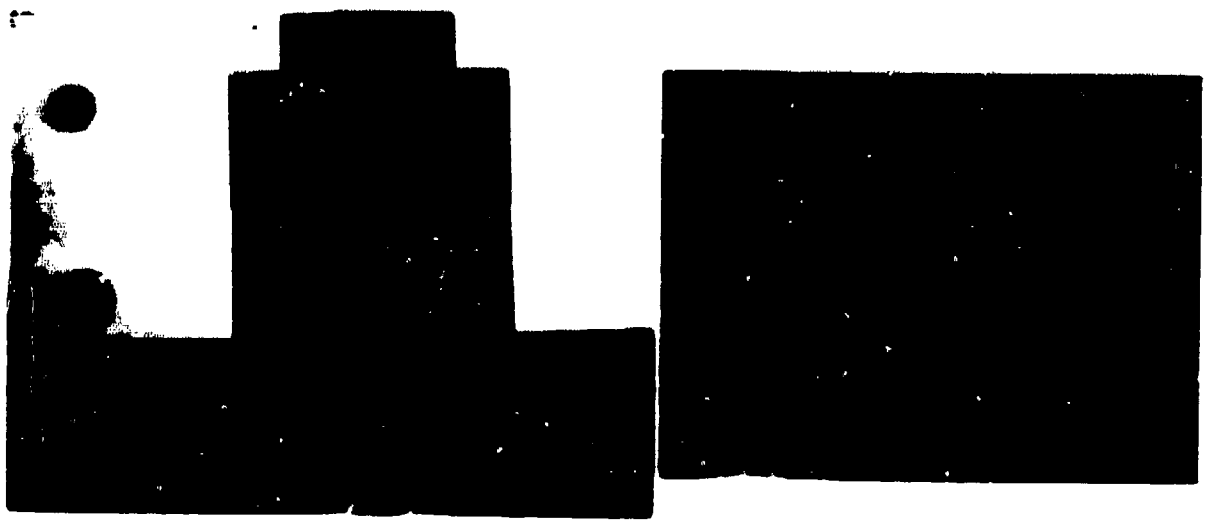

2064

FIG. A-4 ORIGINAL DATA - TESTS 2044, 2064

APPENDIX B

This section consists of sketches depicting the various models tested during this series. The nominal values of the dimensions were used in the reduction of the data. Measured diameters at various stations are tabulated on each sketch and an estimate of the actual shape is also given.

As the test series progressed, a slight rounding of the tips occurred due to repeated hitting of the nylon-impact mats used to stop the models. No correction was attempted for such rounding.

Early in the test series, the tip of the 60/-43 cusp broke off. During the reduction of data in subsequent tests, it was assumed that water contact occurred as if the tip was intact.

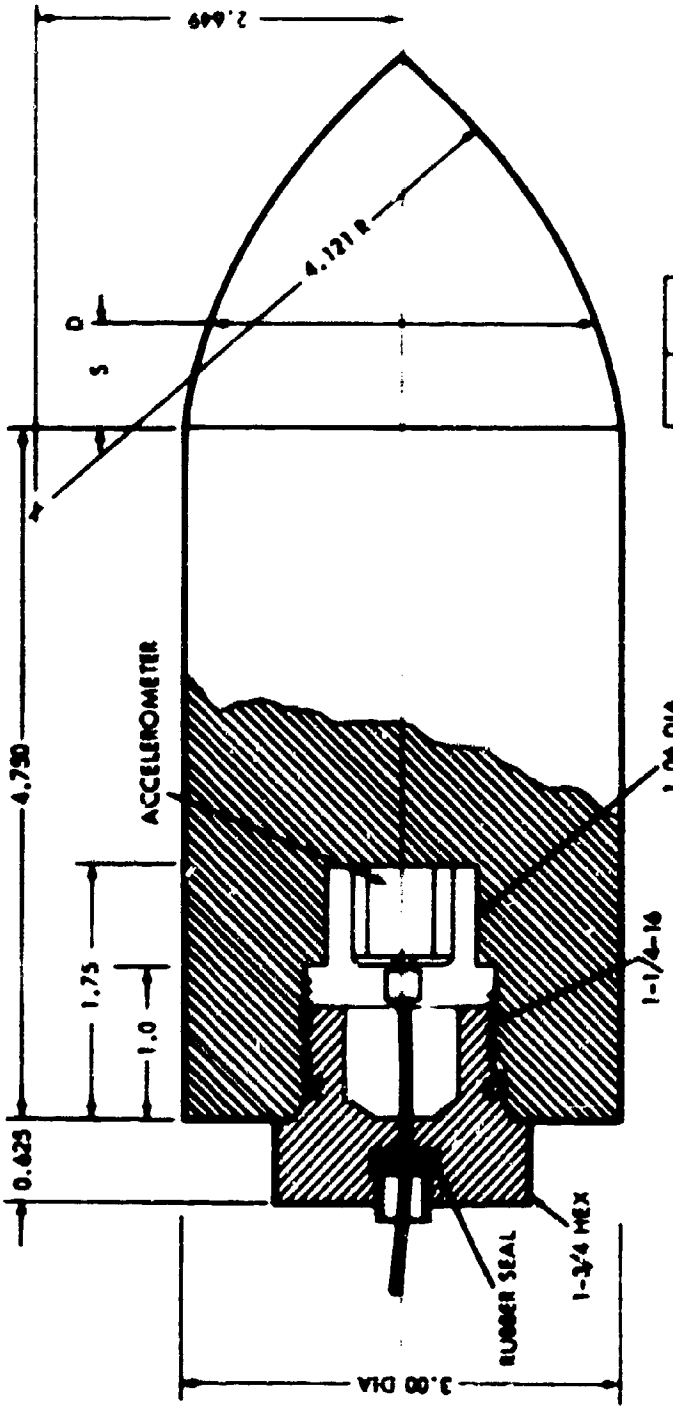

S	D
0	.381 2.649
.754	2.423
1.000	2.431
1.250	2.198
1.750	1.402
2.404	.012

NOTE:
OFFSETS YIELD
APPROX. 40/43

FIG. B-1 40/43 OGIVE MODEL

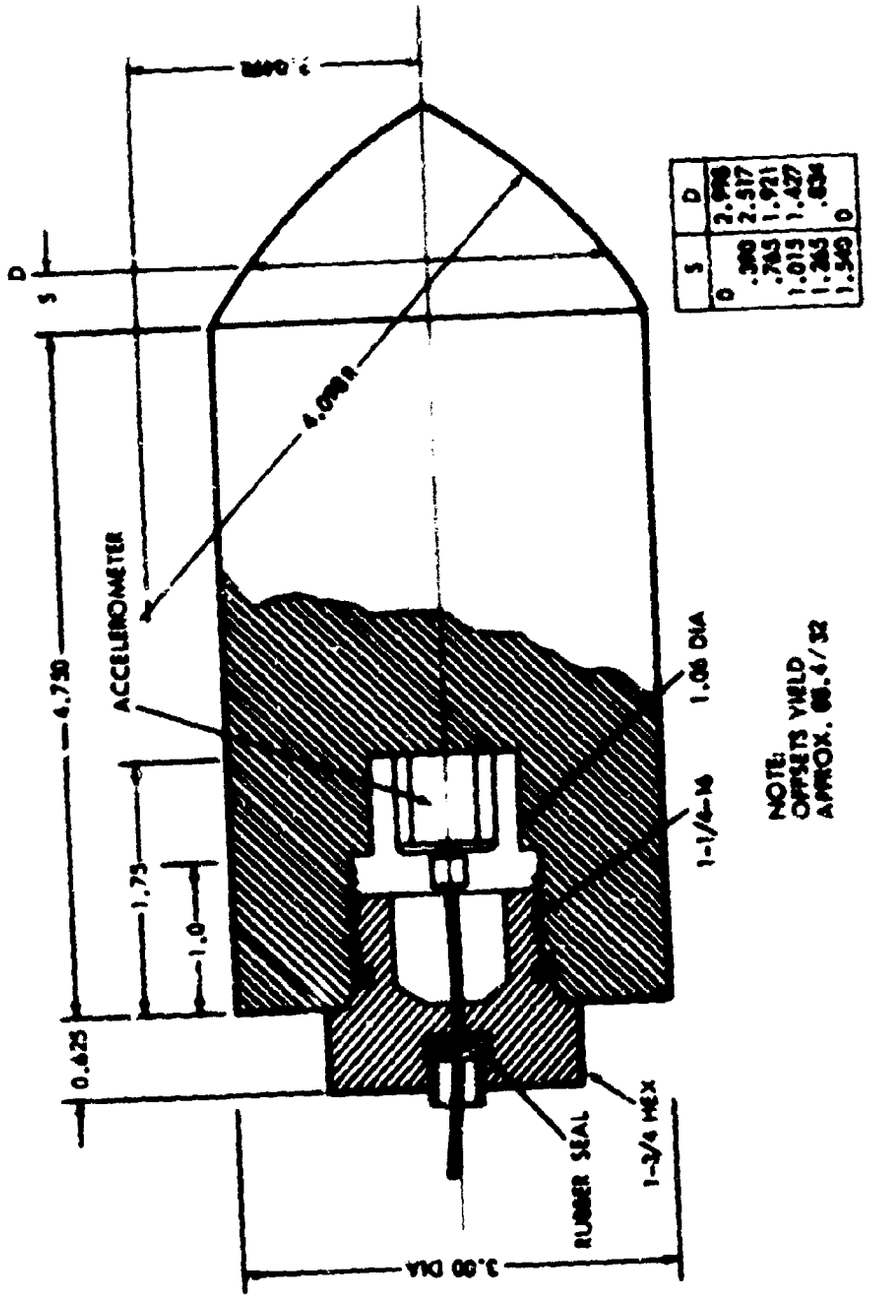

FIG. B-2 10/30 OGIVE MODEL

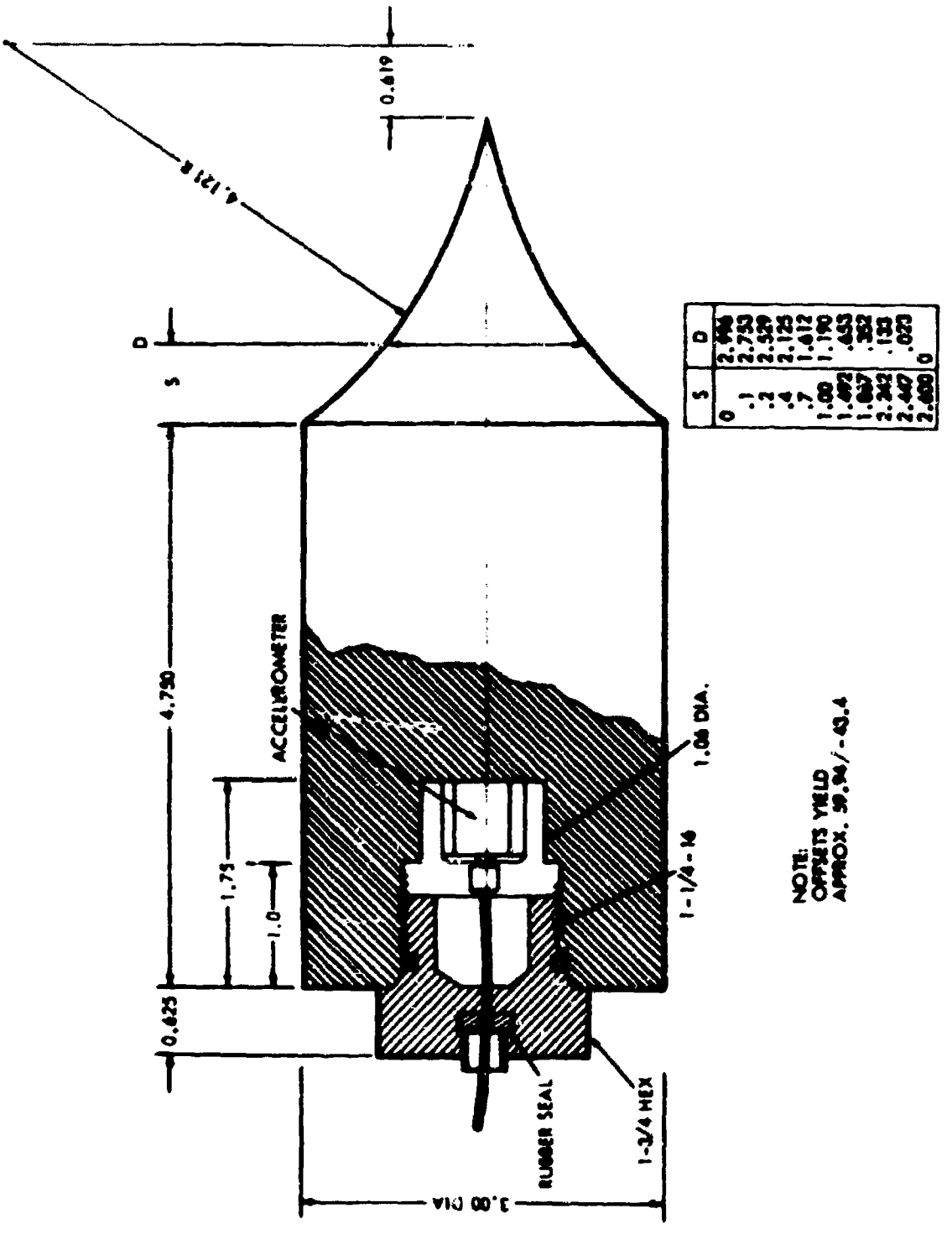

NOTE:
OFFSETS YIELD
APPROX. 59.54/-43.4

FIG. 8-3 60/-43 CUSP MODEL

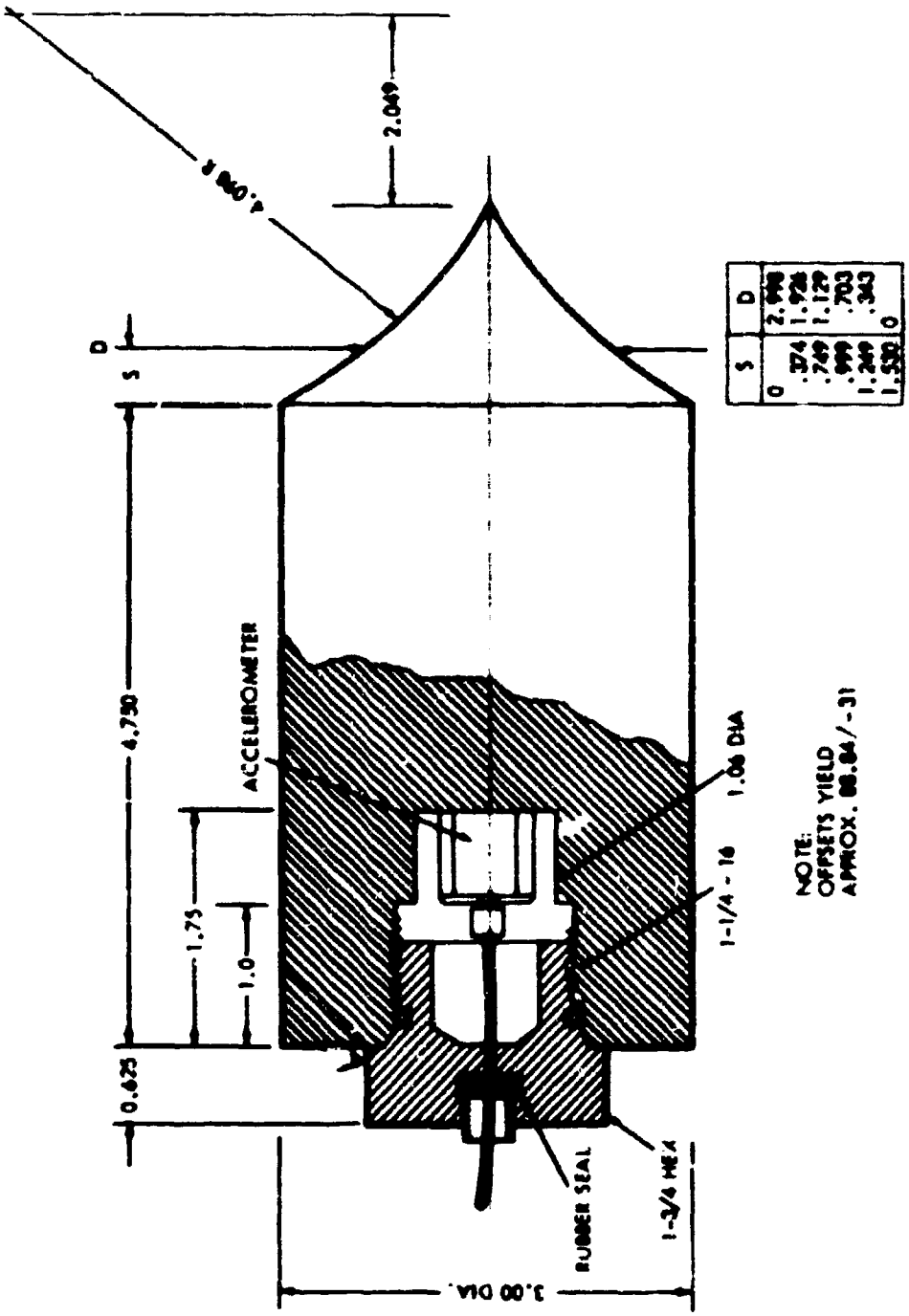

FIG. 8-4 VQ-30 CUSP MODEL

APPENDIX C

This program, written in the BASIC computer language, was used to reduce the data presented in this report. The operations were as follows: (1) the original data is converted into time after entry and acceleration for each data point; (2) the velocity and distance traveled after entry is then computed at the data points using trapezoidal integration; (3) from this basic data, the added mass is determined at each data point by an iterative procedure, as is the distance associated with the maximum total drag coefficient; (4) the values of velocity acceleration and time are then obtained by interpolation at fixed distances relative to the point of maximum total drag coefficient; and (5) the values of total drag coefficient and added mass are then computed at these fixed distances and the results printed.

The subroutines of this program, in order of operation, are:

SUB 500	Reads the data and computes the time acceleration velocity and distance for each data point.
SUB 1400	Computes the buoyancy at each point, assuming no separation.
SUB 900	Defines the initial total mass as the mass of the model and goes to SUB 1000.
SUB 1000	Computes at each point the total drag coefficient, the steady-state drag coefficient (D9), and the data point number associated with the maximum total drag coefficient (E).
SUB 830	Computes the added mass and total mass at each point.
SUB 2000	Converts by interpolation time, velocity, and acceleration from the read points to points fixed relative to the distance associated with the maximum total drag coefficient.
SUB 8000	First print.
SUB 9000	Second print.

The inputs required for this program beginning at line 1700 are:

C1 = Scope swept (sec/cm)
C2 = Scope amplitude (volts/cm)
C3 = Gage constant ($ft/sec^2/volt$)
C4 = Time constant (seconds)
V1 = Entry velocity (ft/sec)
D2 = Water distance (inches)
K2 = Number of data point pairs
C5 = Shot number
D1 = Diameter (ft)
W1 = Weight (lbs)
P1 = Cone angle (degrees)
P2 = Entry angle (degrees)
R1 = Radius of curvature (ft)
B1 = Swept angle (degrees)
U2 = Shape Code: +1 = ogive; -1 = cusp
C6 = Conversion factor (counts per cm)

The data read from the oscilloscope trace are entered as follows: (1) the time coordinate of each data point is entered beginning with line 1730; and (2) the amplitude coordinate of each data point is entered beginning with line 1740.

A sample run is given on pages C-3 and C-4. The program list is given on pages C-5 through C-8.

1400
E= 20
E= 20
E= 20
E= 20
.2000
S(E) .079943
2000
1400
E= 16
E= 16
E= 16
E= 16

SHOT NUMBER 21413 VELOCITY 24.6

DIST	VEL	TIME	ACCEL
.000012	24.6	3.45729E-8	32.7817
6.39664E-2	24.6064	2.16706E-4	27.8293
.127921	24.6115	4.33235E-4	16.8837
.191875	24.6141	6.49763E-4	4.06893
.25583	24.6126	8.66290E-4	-18.8415
.319784	24.6066	1.08285E-3	-34.2024
.383738	24.5973	1.29949E-3	-52.0416
.447693	24.5836	1.51627E-3	-69.2787
.511647	24.567	1.73309E-3	-88.1189
.575602	24.5459	1.95013E-3	-103.994
.639556	24.5222	2.16740E-3	-112.611
.70351	24.497	2.38481E-3	-121.155
.767465	24.4698	2.60249E-3	-128.429
.831419	24.4414	2.82041E-3	-132.536
.895374	24.4123	3.03859E-3	-134.037
.959328	24.383	.003257	-134.51
1.02328	24.3537	3.47573E-3	-133.753
1.08724	24.3249	3.69475E-3	-130.159
1.15119	24.297	3.91396E-3	-124.14
1.21515	24.2706	4.13340E-3	-115.272
1.2791	24.2465	4.35312E-3	-105.356
1.40701	24.2033	4.79313E-3	-92.3357
1.53492	24.1645	5.23391E-3	-83.8862
1.66283	24.1291	5.67559E-3	-78.862
1.79074	24.0948	6.11756E-3	-74.9429
1.91864	24.0628	6.56068E-3	-72.3867
2.04655	24.0307	7.00349E-3	-69.9323
2.17446	24.0003	7.44768E-3	-65.0374
2.49483	23.927	8.56003E-3	-64.1973
2.81401	23.8565	9.67450E-3	-61.3484
3.13378	23.7885	1.07947E-2	-60.5501
3.45355	23.7211	1.19156E-2	-59.4915
3.77332	23.6549	1.30404E-2	-58.0674
4.09309	23.59	1.41693E-2	-57.2253
4.41287	23.5258	1.53008E-2	-56.4865
4.73264	23.4622	1.64352E-2	-55.6727
5.05241	23.3987	1.75722E-2	-55.3982
5.37218	23.3353	1.87129E-2	-55.7203

DIST	DRAG C	ADD M
.000012	-2.23494E-3	-7.94375E-7
6.39664E-2	1.71571E-2	2.75548E-2
.127921	6.00953E-2	.17069
.191875	.11035	.486497
.25583	.200292	1.06206
.319784	.260755	1.9163
.383738	.3312	3.0131
.447693	.399631	4.3672
.511647	.474802	5.98738
.575602	.538813	7.86543
.639556	.574476	9.92817
.70351	.610159	12.1231
.767465	.641103	14.4415
.831419	.659606	16.8515
.895374	.667746	19.3108
.959328	.671768	21.7927
1.02328	.670786	24.2802
1.08724	.658136	26.7425
1.15119	.63535	29.1391
1.21515	.600531	31.429
1.2791	.56097	33.5811
1.40701	.508964	37.5459
1.53492	.475055	41.1923
1.66283	.45492	44.6385
1.79074	.438745	47.9501
1.91864	.428932	51.1654
2.04655	.419019	54.3076
2.17446	.411335	57.3847
2.49423	.395568	64.8599
2.81401	.383647	72.0787
3.13378	.3804	79.1569
3.45355	.375894	86.1633
3.77332	.3696	93.0697
4.09309	.36376	99.8822
4.41287	.36201	106.624
4.73264	.358362	113.298
5.05241	.356865	119.924
5.37218	.358139	126.548

**READY.

```
LIST

SEC464     10.51.12. 09/27/72
10      DIM A(40),B(40),C(40),D(40),E(40),F(40)
12      DIM M(40),N(40),R(40),S(40),T(40),U(40),V(40),X(40),Y(40)
60      U4=-1
100     GO SUB 500
103     GO SUB 1400
106     GO SUB 900
107     GO SUB 830
108     GO SUB 1000
109     GO SUB 830
112     GO SUB 1000
115     GO SUB 830
116     GO SUB 1000
117     GO SUB 830
118     GO SUB 1000
119     IF U4>0 THEN 130
120     GO SUB 2000
121     K8=1
122     K2=E2
123     LET U4=2
125     GO TO 103
130     GO SUB 8000
135     GO SUB 9000
500     READ C1,C2,C3,C4
505     READ V1,D2,K2,C5
508     READ D1,W1,P1,P2
509     READ R1,B1,U2,C6
511     LET A(1)=0
512     LET T(1)=0
515     LET P2=P2/57.3
517     LET W9=W1*SIN(P2)
520     FOR K=1 TO K2
530     READ X(K)
531     NEXT K
532     FOR K=1 TO K2
535     READ Y(K)
538     NEXT K
539     FOR K=2 TO K2
540     LET T(K)=(X(K)-X(1))*C1/C6
560     LET A(K)=(Y(K)-Y(1))*C2*C3/C6
570     LET C(K)=C(K-1)+(A(K)+A(K-1))*(T(K)-T(K-1))/(2*C4)
580     NEXT K
590     LET C9=(-W1+SQR((V1)^2+5.366*D2))/32.2
600     K8=1
610     FOR K=1 TO K2
620     LET A(K)=-A(K)-C(K)+32.2*SIN(P2)
630     T(K)=T(K)-C9
640     IF T(K)>0 THEN 660
650     K8=K8+1
660     NEXT K
```

```
670   LET T(KB-1)=0
671   LET S(KB-1)=0
672   LET V(KB-1)=V1
680   FOR K=KB TO K2
690   V(K)=V(K-1)+.5*(A(K)+A(K-1))*(T(K)-T(K-1))
700   S(K)=S(K-1)+.5*(V(K)+V(K-1))*(T(K)-T(K-1))
710   NEXT K
720   RETURN
830   LET X(KB-1)=0
832   LET Y(KB-1)=0
835   FOR K=KB TO K2
840   X(K)=.761*D1^2*U(K)
850   Y(K)=Y(K-1)+.5*(X(K)+X(K-1))*(S(K)-S(K-1))
858   LET M(K)=Y(K)+W1/32.2
860   NEXT K
865   PRINT "E="E
870   RETURN
900   FOR K=1 TO K2
910   LET M(K)=W1/32.2
920   NEXT K
1000  FOR K=KB TO K2
1010  LET U(K)=((M(K)*(-1)*A(K))+W9-B(K))
1011  LET U(K)=U(K)/(.969+.7854*W(K)^2*(D1)^2)
1020  NEXT K
1025  LET U(KB-1)=0
1030  FOR K=KB TO K2-1
1040  IF U(K)<.1 THEN 1080
1050  IF U(K)-U(K+1)<0 THEN 1080
1060  LET E=K
1070  GO TO 1110
1080  NEXT K
1110  RETURN
1400  PRINT 1400
1410  T3=(P1+(U2*B1))/(2*57.3)
1420  Y1=R1*SIN(T3)
1430  U3=-1
1440  FOR K=KB TO K2
1450  IF U3>0 THEN 1480
1460  R(K)=U2*SQR(R1^2-(Y1-U2*S(K))^2)-U2*(R1*COS(T3))
1470  IF R(K)<.5*D1 THEN 1500
1480  R(K)=.5*D1
1490  U3=6
1500  NEXT K
1510  LET G(KB-1)=0
1515  LET R(KB-1)=0
1520  FOR K=KB TO K2
1530  B(K)=B(K-1)+3.1416*62.4*.5*(R(K)^2+R(K-1)^2)*(S(K)-S(K-1))
1537  LET B(K)=E(K)*SIN(P2)
1540  NEXT K
1550  RETURN
```

```
1700  DATA .005,.05,2809,.075
1710  DATA 24.6,.975,39,81413
1720  DATA .25,3.641,90,90
1721  DATA .3298,30
1725  DATA 1,306
1730  DATA 594,761,796,812,823,831,836,842,849,862,872,881
1731  DATA 898,908,920,937,951,965,978,995,1010,1028,1043
1732  DATA 1055,1070,1092,1120,1164,1230,1296,1388,1500
1733  DATA 1583,1698,1840,1980,2206,2338,2590
1740  DATA 276,276,275,288,311,322,330,360,388,420,449,475
1741  DATA 521,560,576,599,617,627,630,630,627,614,594,573
1742  DATA 549,529,509,491,475,463,451,444,437,430,422
1743  DATA 419,413,408,402
2000  PRINT 2000
2005  PRINT "S(E)"S(E)
2010  LET E3=1
2020  FOR J=K8 TO K2
2030  IF E3=1 THEN 2120
2040  IF E3=2 THEN 2100
2050  IF E3=3 THEN 2080
2080  LET Y(J)=V(J)
2090  GO TO 2130
2100  LET Y(J)=T(J)
2110  GO TO 2130
2120  LET Y(J)=A(J)
2130  NEXT J
2150  FOR J=K8 TO K2-2
2160  LET S2=(J+2)-S(J)
2170  LET S1=S(J+1)-S(J)
2180  LET A1=Y(J+1)-Y(J)
2190  LET A2=Y(J+2)-Y(J)
2200  LET A(J)=((S2*S2*A1)-(S1*S1*A2))/((S1*S2*S2)-(S2*S1*S1))
2210  C(J)=(S2*A1-S1*A2)/(S1↑2*S2-S2↑2*S1)
2220  NEXT J
2230  LET E9=S(E)/15
2240  LET D(1)=.000001
2250  FOR I=2 TO 21
2260  LET D(I)=D(I-1)+E9
2270  NEXT I
2280  FOR I=22 TO 28
2290  LET D(I)=D(I-1)+2*E9
2300  NEXT I
2310  FOR I=29 TO 39
2320  LET D(I)=D(I-1)+5*E9
2330  NEXT I
```

```
2340  FOR J=K8 TO K2-2
2350  IF J>K8+.1 THEN 2380
2360  FOR I=1 TO 39
2370  IF J=K2-2 THEN 2400
2380  IF D(I)>S(J+1) THEN 2520
2390  IF J=E-1 THEN 2630
2400  LET E(I)=(Y(J)+A(J)*(D(I)-S(J))+C(J)*(D(I)-S(J))↑2)
2410  IF D(I)>S(K2)THEN 2530
2420  IF E3=3 THEN 2490
2430  IF E3=2 THEN 2470
2440  IF E3=1 THEN 2450
2450  LET X(I)=E(I)
2460  GO TO 2510
2470  LET T(I)=E(I)
2480  GOTO 2510
2490  LET V(I)=E(I)
2500  GO TO 2510
2510  NEXT I
2520  NEXT J
2530  LET E3=E3+1
2540  IF E3=4 THEN 2570
2550  LET E2=I-1
2560  GO TO 2020
2570  PRINT "2000"
2580  FOR J=1 TO E2
2590  S(J)=D(J)
2600  LET A(J)=X(J)
2610  NEXT J
2620  RETURN
2630  E(I)=Y(J)+(D(I)-S(J))*(Y(J+1)-Y(J))/(S(J+1)-S(J))
2640  GO TO 2410
8000  PRINT
8004  PRINT "SHOT NUMBER "C5, "  VELOCITY "V1
8006  PRINT
8008  PRINT "DIST","VEL","TIME","ACCEL"
8010  FOR K=K8 TO K2
8015  LET D(K)=S(K)*12
8020  PRINT D(K),V(K),T(K),A(K)
8030  NEXT K
8900  RETURN
9000  PRINT
9005  PRINT "DIST","DRAG C","ADD M"
9010  FOR K=K8 TO K2
9015  X(K)=454*(32.2*M(K)-W1)
9020  PRINT D(K),U(K),X(K)
9030  NEXT K
9999  END
**READY.
```

APPENDIX D

In this appendix, there are tabulated numerical results obtained for each test in this series. Also included are plots of average values of total drag coefficient vs depth and added mass vs depth for each shape tested.

In those cases where the tabulated number is not dimensionless, the property list is for a 3-inch-diameter body.

In Table D-1 the column headings have the following meanings: Weight, the model weight with no allowance for the trailing cable; Velocity, the model velocity at the instant of water contact; Depth, the distance traveled from water contact until the maximum total drag coefficient is racked; Cd, the maximum total drag coefficient (friction is included); Added Mass, the computed value of added mass that occurred when the total drag coefficient was maximum; Steady State Drag, the value of the total drag coefficient averaged over the three deepest points.

In Tables D-2 through D-5, the instantaneous values of Total Drag Coefficient and Added Mass in grams are given for selected computing stations. The depth given is the average depth of the computing station and applies to both parts of the table.

Table D-1

Summary of Data

60/43 Ogive

Shot No.	Weight lb	Velocity (ft/sec)	Depth at C_d Max	C_d Max	Added Mass at C_d Max
2055	4.34	12.6	1.15	.308	12.4
2053	4.34	13.6	1.12	.304	11.6
21408	4.09	20.6	1.09	.307	11.2
21409	4.09	24.2	1.08	.292	10.8
2073	4.34	69.8	1.02	.298	12.4
2072	4.34	70.0	1.10	.292	11.5
2071	4.34	71.6	1.09	.314	13.1
Average			1.09	.302	11.9

90/30 Ogive

2052	3.64	13.5	.946	.732	25.7
2051	3.64	13.6	.930	.663	20.8
21412	3.64	24.2	1.052	.665	23.3
21413	3.64	24.6	.959	.672	21.8
2069	3.89	71.0	1.035	.707	27.4
2070	3.89	75.3	.955	.656	24.1
2068	3.89	76.1	1.010	.648	26.7
Average			.991	.678	24.3

60/-43 Cusp

2047	3.57	12.3	2.19	1.45	29.7
2046	3.57	12.9	2.21	1.60	37.6
2048	3.57	13.3	2.22	1.48	33.0
21407	3.57	19.0	-	1.56	29.6
21503	3.57	23.9	2.24	1.49	28.6
2067	3.81	67.8	2.12	1.43	28.9
2066	3.81	67.0	2.21	1.46	29.9
2065	3.81	79.9	2.27	1.47	29.6
Average			2.21	1.49	30.9

90/-30 Cusp

2044	3.46	13.2	1.29	2.45	36.7
2043	3.46	13.6	1.32	2.41	38.1
2042	3.46	13.6	1.33	2.33	35.2
2045	3.46	13.7	1.33	2.29	36.2

Table D-1 (Continued)

Summary of Data

90/-30 Cusp

Shot No.	Weight (lbs)	Velocity (ft/sec)	Depth at C_d Max	C_d Max	Added Mass at C_d Max
21410	3.57	23.14	1.24	2.45	36.1
21411	3.46	24.27	1.24	2.36	34.2
2064	3.70	69.7	1.31	2.40	34.9
2063	3.70	72.2	1.28	2.35	33.2
Average			1.29	2.38	35.6

Table D-2
60/43 Ogive

Total Drag Coefficient

Shot No.	Station 3	6	9	12	15	16	17	19	21	25	29	31
2055	.026	.147	.228	.284	.306	.308	.307	.300	.288	.204	.165	.164
2053	.033	.126	.217	.271	.298	.304	.303	.294	.277	.200	.187	.168
21408	.028	.122	.215	.274	.301	.307	.304	.294	.279	.187	.137	.122
21409	.031	.124	.209	.263	.289	.292	.291	.287	.273	.206	.167	.144
2073	.095	.183	.252	.282	.297	.298	.296	.287	.275	.210	.168	-
2072	.041	.136	.217	.267	.289	.292	.291	.283	.271	.206	.165	-
2071	.065	.160	.260	.298	.313	.314	.311	.303	.289	.211	.177	-
Average	.045	.143	.228	.277	.299	.302	.300	.293	.279	.203	.167	.149
Average Distance	.145	.363	.581	.800	1.02	1.09	1.16	1.31	1.45	2.03	2.83	4.29

Added Mass

Shot No.	3	6	9	12	15	16	17	19	21	25	29	31
2055	-.041	1.15	3.69	7.12	11.1	12.4	13.8	16.5	19.1	27.9	36.6	51.1
2053	.104	1.12	3.37	6.57	10.3	11.6	12.9	15.5	18.0	26.3	35.2	51.1
21408	.076	.99	3.13	6.24	9.89	11.2	12.4	14.9	17.3	25.2	32.4	43.7
21409	.093	1.05	3.16	6.14	9.64	10.9	12.1	14.5	16.8	24.8	33.2	46.4
2073	.439	2.08	4.66	7.84	11.2	12.4	13.6	15.9	18.1	25.7	33.6	-
2072	.145	1.26	3.55	6.69	10.3	11.5	12.7	15.2	17.6	25.6	34.1	-
2071	.298	1.71	4.36	7.88	11.8	13.1	14.4	17.0	19.5	27.9	33.6	-
Average	.159	1.34	3.70	6.93	10.6	11.9	13.1	15.6	18.1	26.2	34.1	48.0

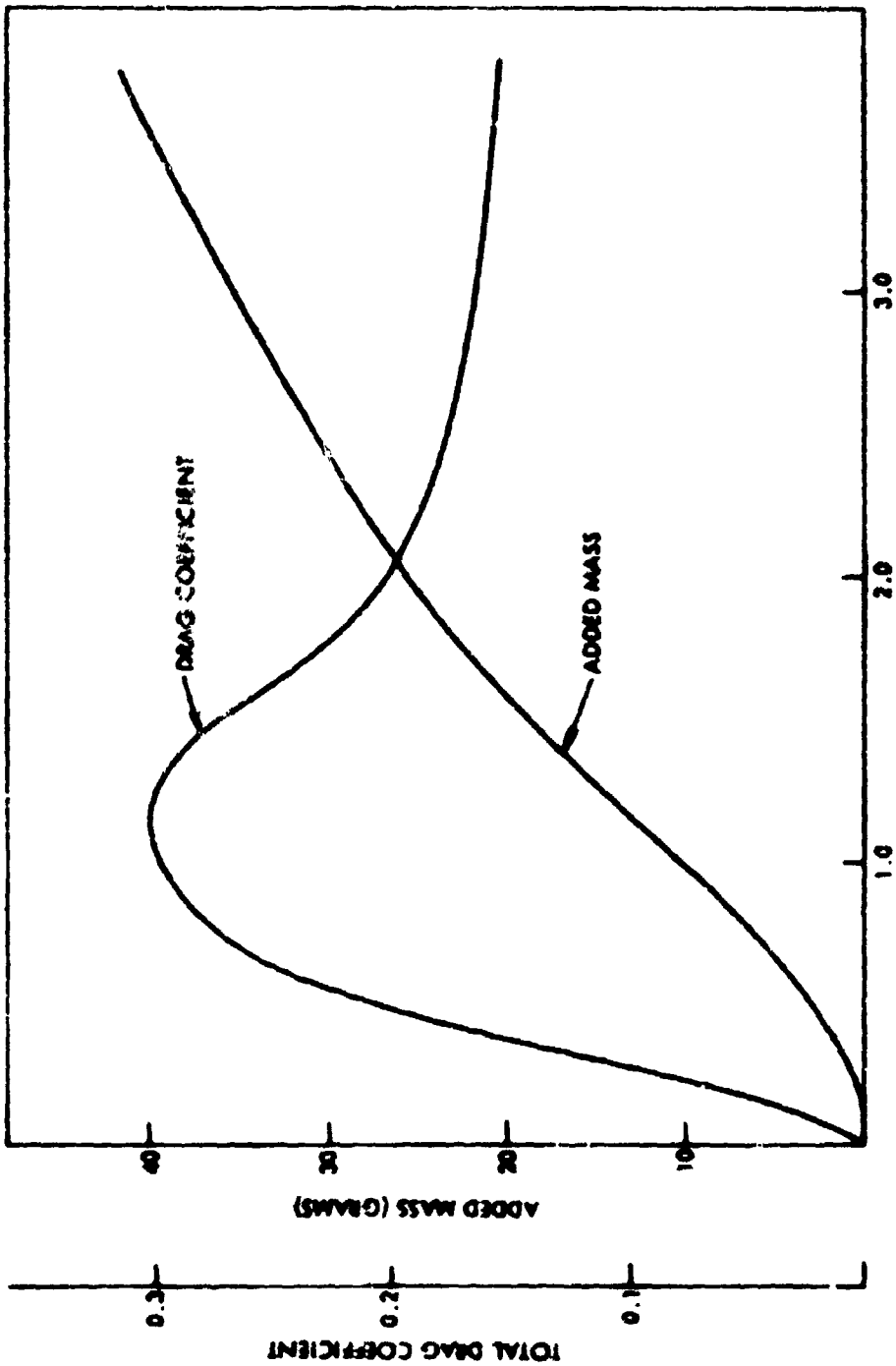

FIG. D-1 AVERAGE TOTAL DRAG COEFFICIENT AND ADDED MASS VS DEPTH FOR 60/43 OGIVES

Table D-3
90/30 Ogive

Total Drag Coefficient

Shot No.	Station 3	6	9	12	15	16	17	19	21	25	29	33
2052	.132	.348	.574	.683	.727	.732	.731	.708	.646	.519	.465	-
2051	.080	.279	.451	.572	.657	.663	.662	.651	.604	.449	.394	.333
21412	.041	.260	.463	.599	.659	.665	.664	.631	.554	.445	.418	.381
21413	.061	.261	.480	.612	.668	.672	.671	.637	.559	.438	.395	.370
2069	.154	.357	.562	.661	.706	.707	.702	.648	.559	.490	.454	-
2070	.154	.352	.525	.615	.650	.656	.656	.622	.565	.455	.417	-
2068	.101	.354	.525	.623	.647	.648	.635	.568	.519	.449	.426	-
Average	.103	.316	.511	.624	.673	.678	.674	.638	.573	.464	.424	.367
Average Distance	.132	.330	.528	.727	.925	.991	1.06	1.19	1.32	1.85	2.58	1.90

Added Mass

2052	.46	3.08	8.26	15.2	23.0	25.7	28.3	33.6	38.5	55.1	74.8	
2051	.163	2.16	6.14	11.7	18.4	20.8	23.2	27.9	32.4	47.0	63.4	89.2
21412	.118	1.90	6.36	12.9	20.6	23.3	26.0	31.3	36.1	51.7	71.1	103.0
21413	.163	1.91	5.97	12.1	19.3	21.8	24.3	29.2	33.6	47.9	64.8	93.0
2069	.62	3.50	8.8	15.7	24.7	27.3	30.0	35.3	42.3	58.8	86.2	-
2070	.589	3.42	8.35	14.7	21.7	24.1	26.6	31.3	35.7	50.3	67.9	-
2068	.354	3.22	8.82	16.2	24.2	26.9	29.7	34.7	39.2	55.2	75.4	-
Average	.352	2.74	7.53	14.1	21.7	24.3	26.9	31.9	36.8	52.3	71.9	96.7

FIG D-2 AVERAGE TOTAL DRAG COEFFICIENT AND ADDED MASS VS DEPTH FOR 90/30 OGIVES

Table D-4
60/-43 Cusp

Total Drag Coefficient

Shot No.	Station 3	6	9	12	15	16	17	19	21	25	29
2047	.029	.022	.032	.234	1.07	1.45	1.11	.807	.683	.567	-
2046	.039	.076	.116	.323	1.14	1.60	1.25	.941	.844	.721	-
2048	.004	.029	.104	.304	1.03	1.48	1.15	.826	.719	.529	-
21407	-.007	.006	.061	.271	1.12	1.56	1.20	.875	.762	.638	-
21503	-.005	.006	.022	.239	1.03	1.49	1.16	.839	.743	.620	.581
2067	.012	.005	.058	.265	1.03	1.43	1.13	.851	.760	-	-
2066	.002	.008	.056	.261	1.03	1.46	1.13	.870	-	-	-
2065	-.001	.013	.060	.254	1.01	1.47	1.14	.880	.744	-	-
Average	.009	.026	.064	.269	1.06	1.49	1.16	.861	.751	.605	.581
Average Distance	.294	.737	1.18	1.62	2.06	2.21	2.36	2.65	2.95	4.13	5.75

Added Mass

2047	.5	1.1	1.8	4.7	19.0	29.7	40.6	56.4	69.0	100.0	-
2046	.4	1.8	4.2	9.0	25.9	37.6	49.8	68.0	83.1	135.0	-
2048	-.04	.4	1.9	6.8	22.3	33.0	44.3	60.9	74.1	116.0	-
21407	-.04	.13	.60	4.1	18.9	29.6	40.6	56.7	69.8	114.5	-
21503	-.13	-.09	.40	3.3	17.7	28.6	40.0	56.8	70.4	116.5	173.2
2067	.27	.37	.99	4.5	18.7	28.9	39.4	55.2	68.3	-	-
2066	.02	.18	.79	4.3	19.2	29.9	41.0	57.8	-	-	-
2065	-.1	.09	.95	4.6	18.7	29.6	41.0	58.5	72.7	-	-
Average	.11	.50	1.5	5.2	20.0	30.9	42.1	58.8	72.4	114.0	173.2

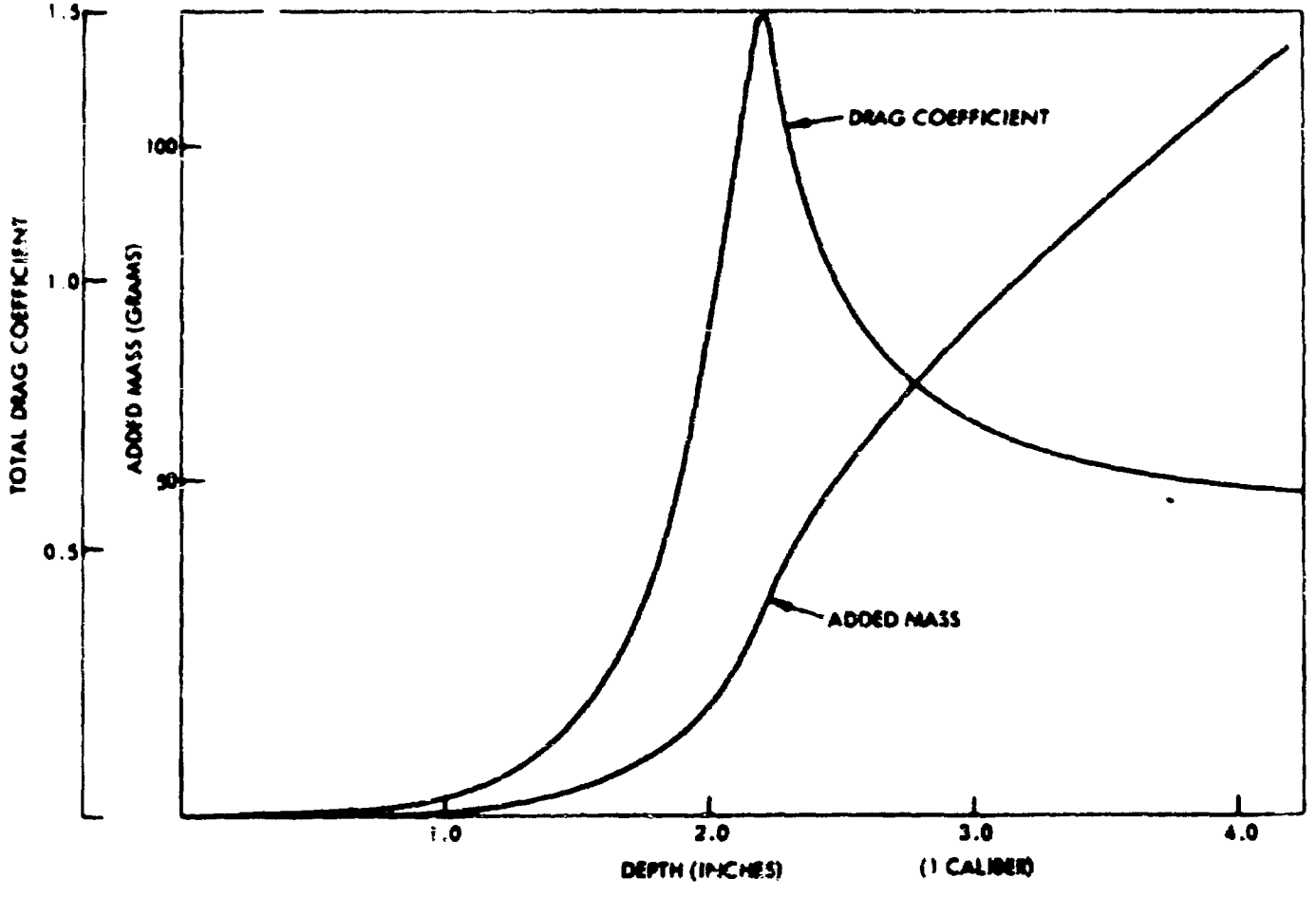

FIG. D-3 AVERAGE TOTAL DRAG COEFFICIENT AND ADDED MASS VS DEPTH FOR 60/-43 CUSPS

Table D-5
90/-30 Cusp

Total Drag Coefficient

Shot No.	Station 3	6	9	12	15	16	17	19	21	25	29	33
2044	.035	.087	.226	.625	1.85	2.45	1.85	1.26	1.10	.866	.760	.676
2043	.055	.080	.224	.626	1.85	2.41	1.72	1.18	1.01	.811	.748	-
2042	.032	.049	.186	.589	1.75	2.34	1.65	1.13	.951	.718	-	-
2045	.056	.100	.218	.594	1.74	2.28	1.73	1.19	1.01	.802	.712	-
21410	.006	.058	.223	.686	1.94	2.45	2.00	1.22	1.06	.844	.766	-
21411	.001	.033	.181	.621	1.92	2.36	1.94	1.20	1.01	.781	.699	-
2064	.001	.040	.178	.608	1.82	2.40	1.70	1.18	1.03	.838	.776	-
2063	.009	.044	.173	.589	1.74	2.35	1.76	1.26	1.04	.841	.782	.775
Average	.024	.061	.201	.617	1.83	2.38	1.79	1.20	1.03	.813	.749	.725
Average Distance	.172	.430	.688	.946	1.20	1.29	1.38	1.55	1.72	2.41	3.35	5.07

Added Mass

2044	.156	1.01	3.17	9.02	26.1	36.7	47.4	62.3	74.0	113	157	227
2043	.476	1.41	3.51	9.52	27.2	38.1	48.7	62.9	74.1	110	154	-
2042	.384	.836	2.49	7.92	24.7	35.2	45.4	59.2	69.9	103	-	-
2045	.436	1.56	3.77	9.31	25.9	36.2	46.6	61.2	72.4	109	151	-
21410	.016	.398	2.18	8.13	25.7	36.1	46.5	60.8	71.5	107	147	-
21411	-.025	.207	1.57	6.90	23.9	34.2	44.6	58.7	69.3	103	144	-
2064	.004	.256	1.73	7.18	24.3	34.9	45.3	59.4	70.5	107	151	
2063	.097	.417	1.83	6.98	23.1	33.2	43.4	58.2	69.4	106	150	227
Average	.		2.53	8.12	25.1	35.6	46.0	60.3	71.4	107	151	227

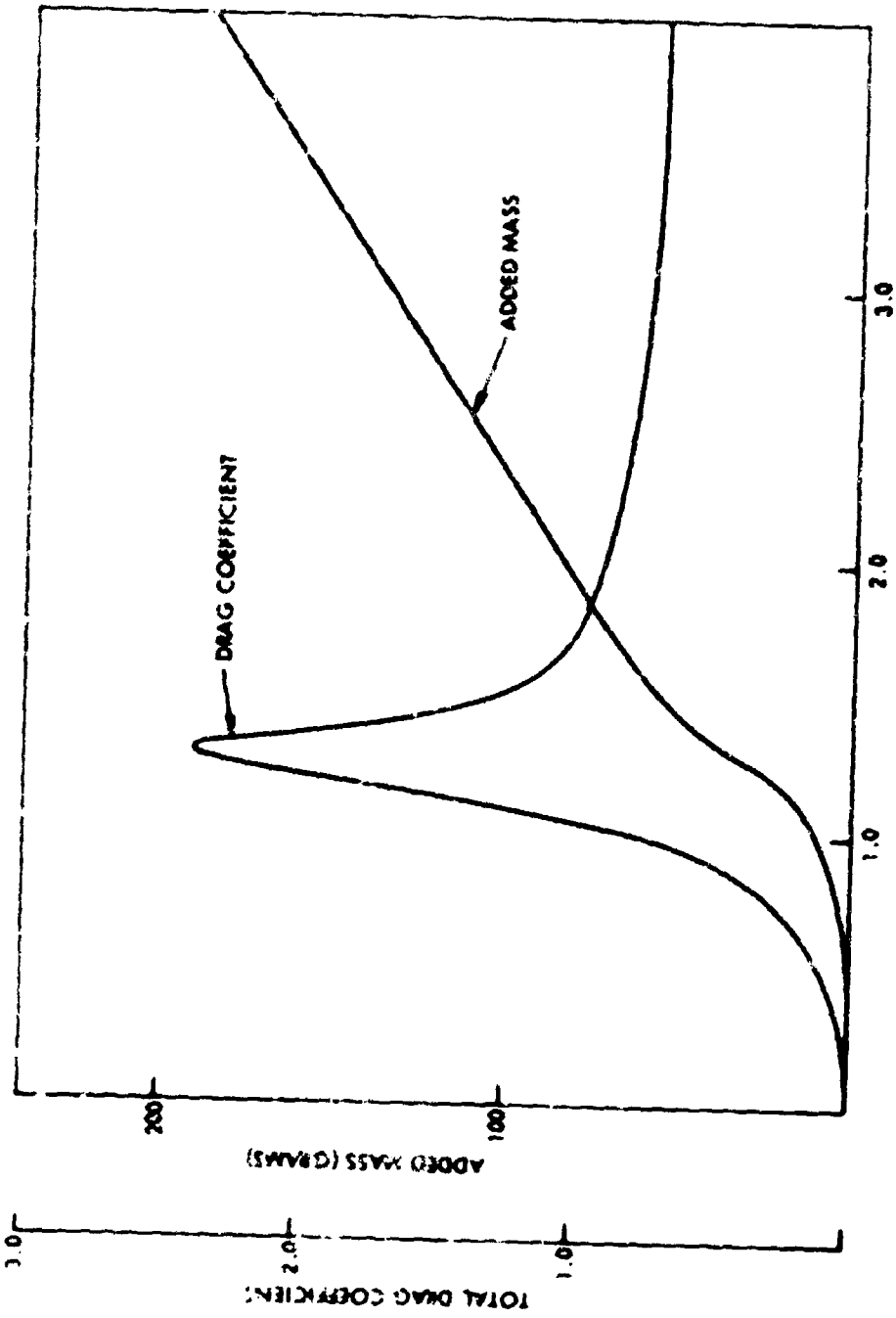

FIG. D-4 AVERAGE TOTAL DRAG COEFFICIENT AND ADDED MASS VS DEPTH FOR 90/-33 CUSPS